Electronic Supplementary Material (ESI) for Journal of Materials Chemistry C.


# Supporting Information

***for***

## Significant Energy Gap Modulation of Sulfone Substituted Benzosiloles: Enhanced Brightness and Electron Affinity for Chemical Vapor Sensing, Fingerprint Detection and Live-Cell Imaging

Gaozhang Gou, Tao Fan, Man Wang, Liangchun Li*

*Shanghai Key Lab of Chemical Assessment and Sustainability, School of Chemical Science and Engineering, Tongji University, Shanghai 200092, P. R. China*

*Corresponding author: E-mail: lilc@tongji.edu.cn

# Content

## 1. Experimental Section

**Materials**. All the experiments were performed in an argon atmosphere employing the standard Schlenk techniques. The starting materials and reagents, which were used as received, were purchased from Adamas, Sigma-Aldrich, J&Kchemical, TCI chemical, Macklin, or Bidepharm. Anhydrous dichloromethane were dried by passing through columns of activated alumina and supported copper catalyst, which is supplied by Shanghai Pucan Laboratory Equipment Co., Ltd. Compounds **3a-S**–**3d-S** and **3e-S**–**3i-S** were synthesized following the reported methods.[S1, S2] Flash column chromatography was performed with silica gel (200–300 mesh). Thin-layer chromatography was carried out on silica gel 60 $F_{254}$ pre-coated plates.

**Instruments and methods**. The $^{1}H$ and $^{13}C$ nuclear magnetic resonance (NMR) measurements were conducted on a Bruker 400 or 600 MHz spectrometer employing tetramethylsilane as an internal standard in $^{1}H$ NMR. The chemical shifts were referenced to the residual non-deuterated solvent peaks ($CDCl_3$: 7.26 and 77.16 ppm for $^{1}H$ NMR and $^{13}C$ NMR, respectively). High-resolution electrospray ionization mass spectrometry (ESI–HRMS) was performed on a Bruker solanX 70 FT–MS spectrometer (the samples were dissolved in HPLC-grade dichloromethane). The measurement error ($\Delta_M$) was calculated from the experimental value ($M_{ex}$) and theoretical value ($M_{th}$) by the equation $\Delta_M = [M_{ex} - M_{th}]/M_{th}$. Infrared (IR) spectroscopy was conducted on a Nicolet 170SX FT–IR spectrophotometer. Further, the morphologies were observed by scanning electron microscopy (SEM, Hitachi S–4800). The ultraviolet–visible (UV–vis) absorption spectra were recorded on a Hitachi U–3010 spectrophotometer. The fluorescent emission spectra were recorded on a Hitachi F–4500 fluorescence spectrophotometer. The fluorescence decay surfaces were determined *via* the single-photon counting technique employing a CD–900 Edinburgh spectrometer. To measure the absolute photoluminescence quantum yield (QY), an F–3018 Integrating Sphere accessory (HORIBA JOBIN YVON) was integrated with the Spex 1681 Flurolog–2 Model F111 spectrophotometer. Cyclic

voltammetry (CV) measurements were conducted on a CHI760E potentiostat which was connected to a three-electrode cell employing glassy carbon, Pt wire and saturated calomel electrode (SEC) as the working, counter and reference electrodes, respectively. The solvents were degassed with argon, and the working electrode was polished with alumina before experiment. The single-crystal X–ray diffraction (SCXRD) data were collected on a Bruker APEX−II CCD diffractometer employing a graphite monochromator with $MoK_{\alpha}$ radiation ($\lambda$ = 0.071073 nm). The density-functional theory (DFT) calculations were conducted with Gaussian16.[S3] Fluorescence microscopy images of labelled cells were obtained with fluorescence microscopy (Nikon ECLIPSE Ti2, Nikon Corporation, Tokyo, Japan). The details of synthetic procedures, photostability test method, cell culture and fluorescence imaging, cytotoxicity study, as well as preparation of the doped material and collection and visualization of latent fingerprints was described below.

**X–ray Diffraction**. Single crystals of **3b**, **3c**, **3f** and **3i** suitable for X–ray diffraction analysis were grown from a mixed solvent of ethanol and dichloromethane. The diffraction data were collected on a Bruker APEX–II CCD diffractometer using a graphite monochromator with MoK$\alpha$ radiation ($\lambda$ = 0.071073 nm) at the preset temperature. The structures were solved by direct methods and refined by full-matrix least-squares methods on all $F^2$ data (Olex2).[S4] Non-hydrogen atoms were refined anisotropically. The positions of hydrogen atoms were calculated and refined isotropically. The crystal data and details of refinements are given in Table S1.

**Electrochemistry**. Cyclic voltammetry experiments were performed with a computer controlled CHI760E electrochemical workstation. Typical electrochemical cells are consisted of three electrode setups including a glassy carbon working electrode, platinum counter electrode, and SCE as quasi-reference electrode. Dichloromethane solutions of the analyte (0.10 $mol \cdot L^{-1}$) and electrolyte (0.10 $mol \cdot L^{-1}$ *n*-$Bu_4NPF_6$) were used for the measurements.[S5] The potentials of the waves were observed in a window of +1.8 to −2.0 V. The HOMO and LUMO energies are derived from the electrochemical data based on $E_{LUMO} = E_{HOMO} + E_g$, $E_{HOMO} = -E_{ox} - 4.74$ eV,

$E_g = E_{HOMO} - E_{LUMO}$.

**Theoretical Calculations**. The popular quantum chemistry software Gaussian 16 package[S3] was used to implement the present computational study. All geometrical structures were fully optimized without the symmetric restraint using the DFT method combined with the Becke, three-parameter, Lee–Yang–Parr (B3LYP) exchange-correlation functional[S6, S7] at the 6–31+G(d, p) basis set. The electronically excited states involving the first 30 excited states were calculated by using the TD–DFT method. In all calculations, squeezed self-consistent field (SCF) convergence standards, the self-consistent reaction field (SCRF) method and polarized continuum model (PCM)[S8] were adopted. The UV–vis spectra were computed from TD–DFT calculations in different states (gas state, $CH_2Cl_2$ solution) and molecular orbitals are calculated in gas state.

**Photostability test**: To determine the photostability of luminogens by photobleaching upon direct irradiation, the following experiment was carried out for representative sulfone modified benzosilole or dithienobenzosilole luminogens.

The luminogens were dissolved in air-saturated $CH_2Cl_2$ ($5.0 \times 10^{-6}$) M in the dark and charged into a sealable quartz cell (10 mm × 10 mm × 50 mm). The absorption and fluorescence spectra were measured to yield the spectra at t = 0 min. The sample was then irradiated using a UV lamp with a 365 nm light (rated power = 8 W, power density = 86.5 mW $cm^{-2}$, calculated by the rated power of UV lamp and the light-emitting area) for 2 min and the absorption, fluorescence spectra at t = 2 min were obtained. During the irradiation process, the quartz cell was fixed perpendicularly to the UV lamp and the distance from the light-facing side of the quartz cell to the UV lamp was 2 cm. By repeating irradiation under the same irradiation condition, UV–vis and fluorescence spectrophotometry spectra after 4, 6, 8, 10, 15, 20, 30 (until 60) minutes of irradiation were acquired.

**Cell culture and Cell fluorescence imaging**. Human cervical cancer cells (HeLa) were obtained from the cell bank of the Shanghai Institute of Biochemistry and Cell Research. The cells ($1 \times 10^6$ cells $mL^{-1}$) were seeded in 6-well plates and incubated in

DMEM (Dulbecco's Modified Eagle Medium) supplemented with 10% FBS (fetal bovine serum) and 100 U $mL^{-1}$ Penicillin-Streptomycin Solution (PS) for 12 h. Cells were then incubated in the presence of **3b**, **3d**, **3e**, **3f**, **3g** and **3i** (10 μM ) for 24 h , respectively. At last, the cells were fixed with 4% paraformaldehyde for 0.5 h and washed with the phosphate buffer saline (PBS). The fluorescence imaging was acquired by a fluorescence microscopy (Nikon ECLIPSE Ti2, Nikon Corporation, To kyo, Japan). The green channel excited at 494 nm and collected in the range of 500–5 30 nm.

**Cytotoxicity study**. MTT assays were performed to assess the metabolic activity of Hela cells. Hela cells were seeded in 96-well plates (Costar, IL, USA) at an intensity of $2 \times 10^4$ cells $mL^{-1}$. Then, the medium was replaced by a solution of **3b**, **3d**, **3e**, **3f**, **3g** and **3i** in different concentration, and the cells were then incubated for 24 h. After the designated time intervals, the wells were washed twice with PBS buffer. And a freshly prepared MTT solution (10 μL, 5 mg $mL^{-1}$) in culture medium was added into each well. The MTT medium solution was carefully removed after incubation for 4 h in the incubator. DMSO (100 μL) was then added into each well and gently shaken for 10 min at room temperature to dissolve all the formed precipitate. The absorption of MTT at 490 nm was monitored by the ELX–800 microplate reader (ELISA Reader). Cell viability was expressed by the ratio of the absorption of the cells incubated with **3b**, **3d**, **3e**, **3f**, **3g** and **3i** solution. The result is an average value from six wells; 100% viability of the untreated cells was used as reference.

**Preparation of hydrogel**. To prepare blank hydrogel (10% w/v), 100 mg of triglycerol monostearate (TG-18) (AK Scientific) was charged into a plastic centrifuge tube, followed by the addition of DMSO–water mixture (1.0 ml, 1 : 4 volume ratio). The mixture was heated to 60–80 ℃ until TG-18 was dissolved. The vial was then placed on a flat surface and allowed to room temperature for 15–30 min, resulting in hydrogel formation. For preparing doped hydrogel, all conditions are the same, except for using **3a**–**3i** DMSO solution (1.0 mg $mL^{-1}$) instead of DMSO, and the doping ratio is 4 wt‰.

**Preparation of the luminogens@diatomite**. The suspension of diatomite (1.0 g) in methanol (100 ml) treated by hydrochloric acid and high temperature calcination, was gently stirred and a solution of **3c**, **3f**, **3g**, **3h** and **3i** (100 μL, 1.0 mM) was added over 2.0 min. After stirring for 2 h, the supernatant solution became colorless indicating the deposition of these luminogens on the diatomite. The suspension was filtered, washed with methanol and dried at 70 $^{o}$C for 2 h before use. The doping ratio of the prepared luminogens@diatomite was only 0.1 wt‰.

**Fingerprint development and imaging**. As far as this study is concerned, fingermarks were collected from one voluntary donors (33 years old) and deposited on different materials (glass slide, zinc plate, copper plate, white ceramic tile, transparent plastic bag, wooden plank and leather) surface. The donor rubbed his right-hand thumb on forehead/nose tip and then it was press-stamped on selected substrates. These fingerprint bearing surfaces were dusted with **3f** or **3i** adsorbed diatomite and then excess powder was blown away with air. The developed fingerprint with **3f**@diatomite or **3i**@diatomite was illuminated with UV lamp (365 nm) and images were taken by a smartphone camera.

## 2. Synthesis and Characterization

**General method: 3x-S** (0.18 mmol) was charged into a two-neck flask equipped with a stirring bar. Anhydrous dichloromethane (20 mL) and *m*-CPBA (8.0 equiv, 288 mg, *ca.* 85%) were added, and the reaction mixture was stirred at 45 ℃ for 12 h. After cooling to room temperature, the reaction mixture was washed with sodium sulfite solution, aqueous $NaHCO_3$, brine, dried over $Na_2SO_4$ and concentrated. The residue was purified by silica gel chromatography (PE : DCM, 1 : 2) to give the desired product **3a**–**3i**.

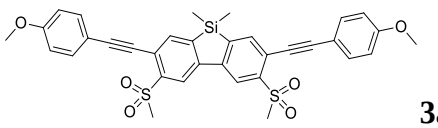

**3a** was obtained as yellow solid (80.0 mg, 72.7%). $^1$H NMR (400 MHz, $CDCl_3$) $\delta$ 8.58 (s, 2H), 7.98 (s, 2H), 7.57 (d, $J$ = 8.8 Hz, 4H),

6.93 (d, $J$ = 8.8 Hz, 4H), 3.85 (s, 6H), 3.35 (s, 6H) ppm. $^{13}$C NMR (101 MHz, $CDCl_3$) $\delta$ 159.74, 144.80, 144.06, 142.32, 137.48, 132.52, 120.98, 120.68, 113.45, 113.37, 99.19, 84.29, 54.55, 41.51, –4.71 ppm. IR (KBr, cm$^{-1}$): 2931, 2205, 1603, 1506, 1449, 1308, 1245, 1137, 1024, 828, 775, 535, 511. HRMS (ESI, m/z): $[M + H]^+$ calculated for $C_{34}H_{30}O_6S_2Si$, 627.1325; found 627.1324, $\Delta_M$: 0.16 ppm.

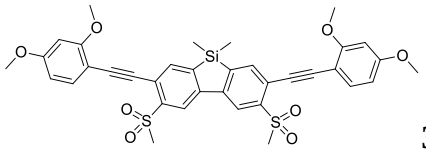

**3b** was obtained as yellow solid (85.1 mg, 69.1%). $^1$H NMR (400 MHz, $CDCl_3$) $\delta$ 8.57 (s, 2H), 7.98 (s, 2H), 7.51 (d, $J$ = 8.4 Hz, 2H), 6.52 (d, $J$ = 8.4 Hz, 2H), 6.48 (s, 2H), 3.91 (s, 6H), 3.85 (s, 6H), 3.44 (s, 6H), 0.52 (s, 6H) ppm. $^{13}$C NMR (101 MHz, $CDCl_3$) $\delta$ 162.38, 161.84, 145.68, 144.85, 143.14, 138.62, 134.82, 122.16, 121.43, 105.43, 104.31, 98.67, 97.01, 89.09, 55.94, 55.71, 42.18, –3.69 ppm. IR (KBr, cm$^{-1}$): 2922, 2195, 1700, 1605, 1566, 1449, 1300, 1205, 1137, 1020, 832, 772, 733, 525. HRMS (ESI, m/z): $[M + H]^+$ calculated for $C_{36}H_{34}O_8S_2Si$, 687.1537; found 687.1533, $\Delta_M$: 0.58 ppm.

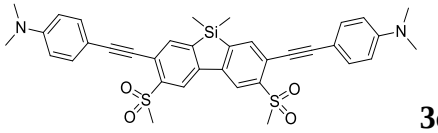

**3c** was obtained as orange solid (91 mg, 78.6%). $^1$H NMR (600 MHz, $CDCl_3$) $\delta$ 8.55 (s, 2H), 7.94 (s, 2H), 7.50 (d, $J$ = 8.7 Hz, 4H), 6.68 (d, $J$ = 8.8 Hz, 4H), 3.36 (s, 6H), 3.03 (s, 12H), 0.52 (s, 6H) ppm. $^{13}$C NMR (101 MHz, $CDCl_3$) $\delta$ 150.96, 145.29, 144.83, 142.80, 138.13, 133.23, 122.45, 121.47, 111.91, 108.77, 102.03, 85.10, 42.39, 40.28, –3.66 ppm. IR (KBr, cm$^{-1}$): 2925, 2178, 1696, 1605, 1531, 1444, 1360, 1302, 1238, 1193, 1135, 944, 808, 783, 760, 667, 511. HRMS (ESI, m/z): $[M + H]^+$ calculated for $C_{36}H_{36}N_2O_4S_2Si$, 653.1958; found 653.1952, $\Delta_M$: 0.92 ppm.

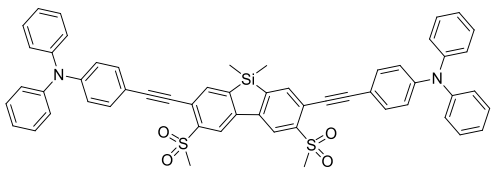

**3d** was obtained as orange solid (122 mg, 75.3%). $^1$H NMR (600 MHz, $CDCl_3$) $\delta$ 8.57 (s, 2H), 7.97 (s, 2H), 7.45 (d, $J$ = 8.5 Hz, 4H), 7.30 (t, $J$ = 7.8 Hz, 8H), 7.14 (d, $J$ = 7.8 Hz, 8H), 7.10 (t, $J$ = 7.4 Hz, 4H), 7.02

(d, $J$ = 8.6 Hz, 4H), 3.35 (s, 6H), 0.53 (s, 6H) ppm. $^{13}$C NMR (101 MHz, $CDCl_3$) $\delta$ 149.15, 147.00, 145.71, 145.01, 143.25, 138.43, 132.89, 129.65, 125.52, 124.19, 122.00, 121.74, 121.66, 114.47, 100.66, 85.75, 42.50, –3.70 ppm. IR (KBr, $cm^{-1}$): 2916, 2199, 1583, 1486, 1313, 1271, 1139, 1082, 1016, 785, 752, 692, 614, 509. HRMS (ESI, m/z): $[M + H]^+$ calculated for $C_{56}H_{44}N_2O_4S_2Si$, 901.2584; found 901.2588, $\Delta_M$: 0.44 ppm.

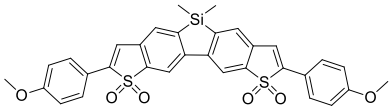

**3e** was obtained as yellow solid (86 mg, 80.4%). $^1$H NMR (600 MHz, $CDCl_3$) $\delta$ 8.17 (s, 2H), 7.80 (d, $J$ = 7.5 Hz, 4H), 7.62 (s, 2H), 7.18 (s, 2H), 7.00 (d, $J$ = 3.2 Hz, 4H), 3.87 (s, 6H), 0.52 (s, 6H) ppm. Owing to the very poor solubility of this compound, $^{13}$C NMR spectrum with satisfactory resolution could not be obtained. IR (KBr, $cm^{-1}$): 2918, 1605, 1508, 1440, 1389, 1296, 1261, 1181, 1139, 1028, 826, 785, 671, 589, 517. HRMS (ESI, m/z): $[M + H]^+$ calculated for $C_{32}H_{26}O_6S_2Si$, 621.0832; found 621.0848, $\Delta_M$: 2.58 ppm.

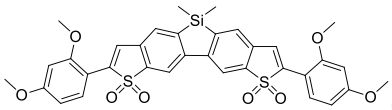

**3f** was obtained as yellow solid (93 mg, 78.8%). $^1$H NMR (600 MHz, $CDCl_3$) $\delta$ 8.11 (s, 2H), 8.07 (d, $J$ = 8.6 Hz, 2H), 7.68 (s, 2H), 7.62 (s, 2H), 6.62 (d, $J$ = 7.9 Hz, 2H), 6.54 (s, 2H), 3.89 (s, 6H), 3.86 (s, 6H), 0.50 (s, 6H) ppm. $^{13}$C NMR (101 MHz, $CDCl_3$) $\delta$ 162.23, 160.21, 147.46, 145.95, 139.32, 138.73, 132.25, 129.59, 128.97, 124.32, 113.97, 109.65, 105.13, 99.62, 55.74, 55.70, –3.66 ppm. IR (KBr, $cm^{-1}$): 2922, 1727, 1607, 1568, 1504, 1449, 1300, 1282, 1214, 1139, 1043, 915, 826, 772, 603, 577. HRMS (ESI, m/z): $[M + H]^+$ calculated for $C_{34}H_{30}O_8S_2Si$, 659.1224; found 659.1221, $\Delta_M$: 0.46 ppm.

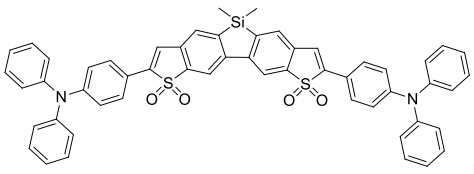

**3g** was obtained as red solid (113 mg, 71.9%). $^1$H NMR (600 MHz, $CDCl_3$) $\delta$ 8.12 (s, 2H), 7.67 (d, $J$ = 8.8 Hz, 4H), 7.60 (s, 2H), 7.31 (t, $J$ = 7.9 Hz, 8H), 7.15 (d, $J$ = 7.6 Hz, 10H), 7.11 (t, $J$ = 7.4 Hz, 4H), 7.08 (d, $J$ = 8.8 Hz, 4H), 0.51 (s, 6H) ppm. $^{13}$C NMR (151 MHz, $CDCl_3$) $\delta$ 149.94, 147.55, 146.84, 146.12,

142.96, 139.82, 131.38, 129.68, 128.78, 127.63, 125.64, 124.37, 122.04, 120.39, 119.85, 114.32, –3.69 ppm. IR (KBr, $cm^{-1}$): 2920, 1717, 1583, 1488, 1284, 1193, 1141, 1073, 822, 785, 750, 694, 583. HRMS (ESI, m/z): $[M + H]^+$ calculated for $C_{54}H_{40}N_2O_4S_2Si$, 873.2271; found 873.2271, $\Delta_M$: 0.00 ppm.

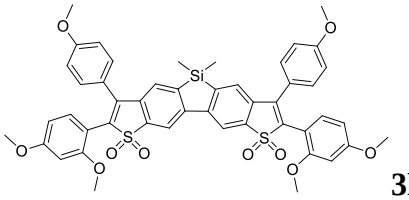

**3h** was obtained as yellow solid (118 mg, 75.6%). $^1H$ NMR (600 MHz, $CDCl_3$) $\delta$ 8.21 (s, 2H), 7.59 – 7.53 (m, 4H), 7.21 (d, $J$ = 8.7 Hz, 4H), 6.86 (d, $J$ = 8.7 Hz, 4H), 6.48 (dd, $J$ = 8.5, 2.3 Hz, 2H), 6.27 (d, $J$ = 2.3 Hz, 2H), 3.76 (s, 6H), 3.74 (s, 6H), 3.33 (s, 6H), 0.35 (s, 6H) ppm. $^{13}C$ NMR (151 MHz, $CDCl_3$) $\delta$ 162.59, 160.20, 159.05, 147.71, 145.71, 140.06, 139.30, 134.35, 133.01, 131.94, 130.03, 127.69, 124.63, 114.68, 114.12, 108.53, 105.13, 99.44, 55.66 – 55.22, –3.65 ppm. IR (KBr, $cm^{-1}$): 2927, 1733, 1603, 1572, 1498, 1457, 1296, 1247, 1207, 1144, 1026, 942, 832, 785, 614, 573. HRMS (ESI, m/z): $[M + H]^+$ calculated for $C_{48}H_{42}O_{10}S_2Si$, 871.2061; found 871.2048, $\Delta_M$: 1.49 ppm.

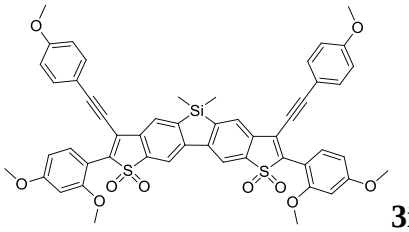

**3i** was obtained as yellow solid (131 mg, 79.3%). $^1H$ NMR (600 MHz, $CDCl_3$) $\delta$ 8.20 (s, 2H), 7.92 (s, 2H), 7.86 (d, $J$ = 8.5 Hz, 2H), 7.45 (d, $J$ = 8.7 Hz, 4H), 6.92 (d, $J$ = 8.7 Hz, 4H), 6.62 (dd, $J$ = 8.6, 2.2 Hz, 2H), 6.58 (d, $J$ = 2.2 Hz, 2H), 3.88 (s, 6H), 3.85 (d, $J$ = 1.4 Hz, 12H), 0.59 (s, 6H) ppm. $^{13}C$ NMR (151 MHz, $CDCl_3$) $\delta$ 163.16, 160.86, 160.00, 148.04, 146.14, 139.73, 138.77, 133.82, 131.35, 131.24, 127.49, 122.11, 114.43, 114.14, 114.07, 109.02, 105.07, 104.24, 99.28, 80.73, 55.69, 55.56, –3.60 ppm. IR (KBr, $cm^{-1}$): 2925, 2191, 1733, 1601, 1568, 1508, 1459, 1292, 1251, 1209, 1146, 1024, 828, 787, 690, 624, 579. HRMS (ESI, m/z): $[M + H]^+$ calculated for $C_{52}H_{42}O_{10}S_2Si$, 919.2061; found 919.2055, $\Delta_M$: 0.65 ppm.

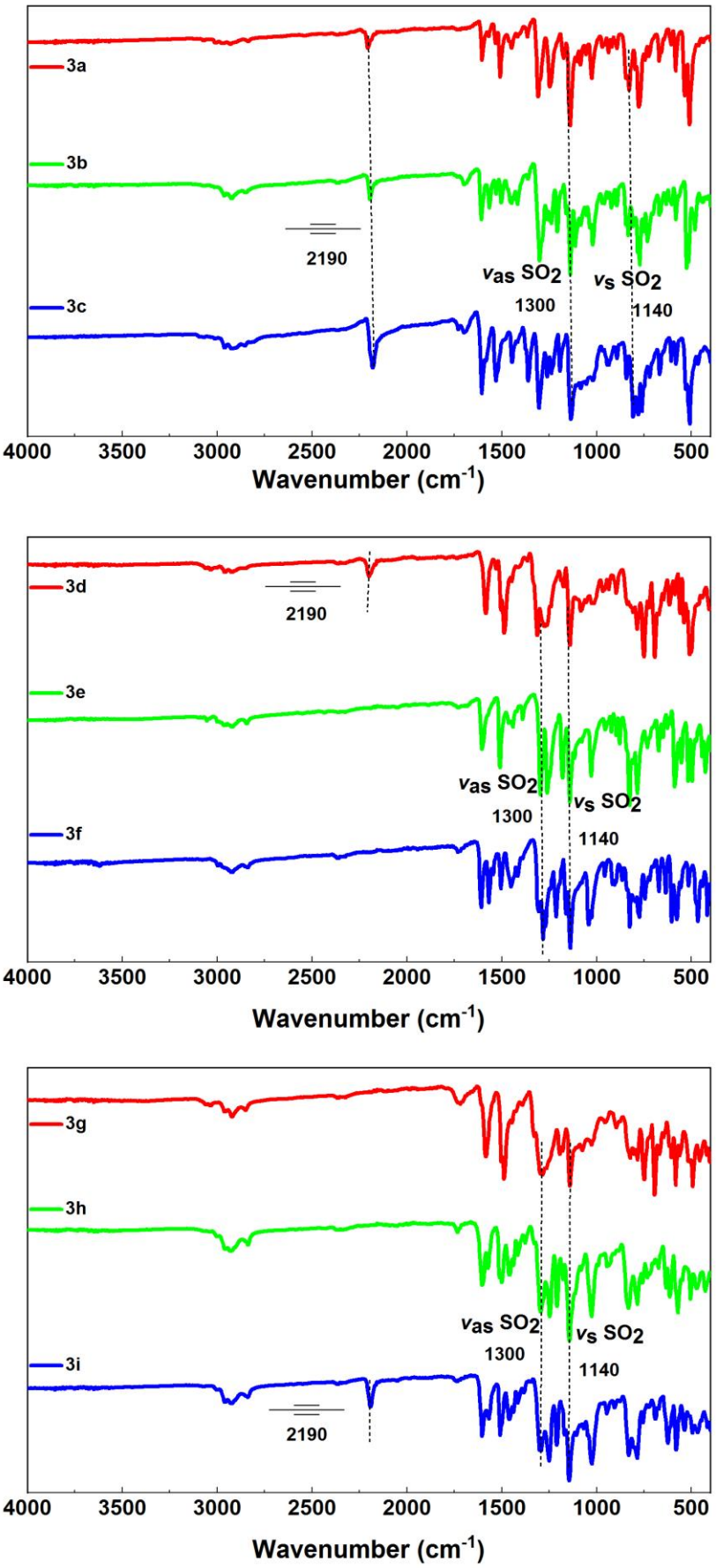


**Fig. S1** The infrared spectroscopy of **3a**–**3i**.

### 3. Crystal structure data

**Table S1** Crystal data of **3b**, **3c**, **3f** and **3i**.

| | **3b** | **3c** | **3f** | **3i** |
|---|---|---|---|---|
| CCDC No. | **2167217** | **2167029** | **2167227** | **2167228** |
| formula | $C_{37}H_{36}Cl_2O_8S_2Si$ | $C_{73}H_{74}Cl_2N_4O_8S_4Si_2$ | $C_{71}H_{66}Cl_6O_{16}S_4Si2$ | $C_{52}H_{42}O_{10}S_2Si$ |
| fw | 771.77 | 1390.68 | 1572.36 | 919.07 |
| color | yellow | orange | yellow | yellow |
| crystal size | 0.15 ×0.13 ×0.1 | 0.15 ×0.1 ×0.05 | 0.12 ×0.11 ×0.1 | 0.2 ×0.1 ×0.08 |
| crystal system | monoclinic | monoclinic | orthorhombic | monoclinic |
| space group | *P2₁/c* | *P2/n* | *Pcca* | *P2₁/n* |
| *a*, Å | 21.237(4) | 12.355(6) | 34.409(6) | 15.339(7) |
| *b*, Å | 16.940(2) | 8.516(4) | 14.0969(13) | 14.970(7) |
| *c*, Å | 21.187(5) | 16.980(9) | 14.8674(18) | 21.442(14) |
| $\alpha$, deg | 90 | 90 | 90 | 90 |
| $\beta$, deg | 112.068(8) | 90.728(15) | 90 | 106.407(14) |
| $\gamma$, deg | 90 | 90 | 90 | 90 |
| *V*, Å$^3$ | 7064(2) | 1786.4(15) | 7211.6(16) | 4723(4) |
| *Z* | 8 | 2 | 4 | 4 |
| *T*, K | 100.0 | 100.0 | 298.15 | 150.0 |
| $D_c$, g cm$^{-3}$ | 1.451 | 1.293 | 1.448 | 1.292 |
| $\mu$, mm$^{-1}$ | 0.389 | 0.298 | 0.454 | 0.197 |
| *F*(000) | 3216.0 | 730.0 | 3256.0 | 1920.0 |
| $2\theta_{max}$, deg | 5.218 to 49.496 | 5.352 to 50.078 | 5.336 to 52.72 | 4.956 to 50.204 |
| *no*. reflections | 154978 | 38618 | 124746 | 52483 |
| *no*. independent reflections | 12032 [*R*(int) = 0.0539] | 3155 [*R*(int) = 0.0570] | 7367 [*R*(int) = 0.0479] | 8374 [*R*(int) = 0.0593] |
| *no*. variables | 917 | 235 | 511 | 595 |
| *GOF* on F$^2$ | 1.034 | 1.092 | 1.026 | 1.034 |
| $R_1{}^a$ | 0.0740 [$I$> 2σ($I$)] | 0.0769 [$I$ > 2σ($I$)] | 0.0643 [$I$ > 2σ($I$)] | 0.0587 [$I$ > 2σ($I$)] |
| $wR_2{}^b$ | 0.2034 | 0.2133 | 0.1652 | 0.1656 |
| residual $\rho$, eÅ$^{-3}$ | +1.89, –1.59 | + 1.26, –1.02 | +1.19, –1.26 | +1.14, –0.36 |

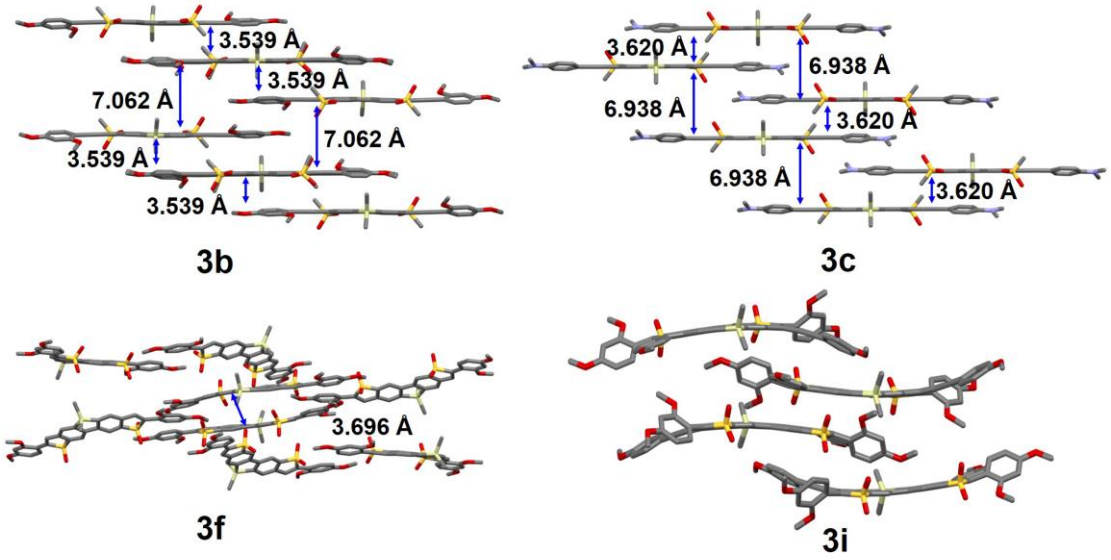


**Fig. S2** The molecular packings of the crystals **3b**, **3c**, **3f** and **3i**.

## 4. Photophysical and electrochemical properties

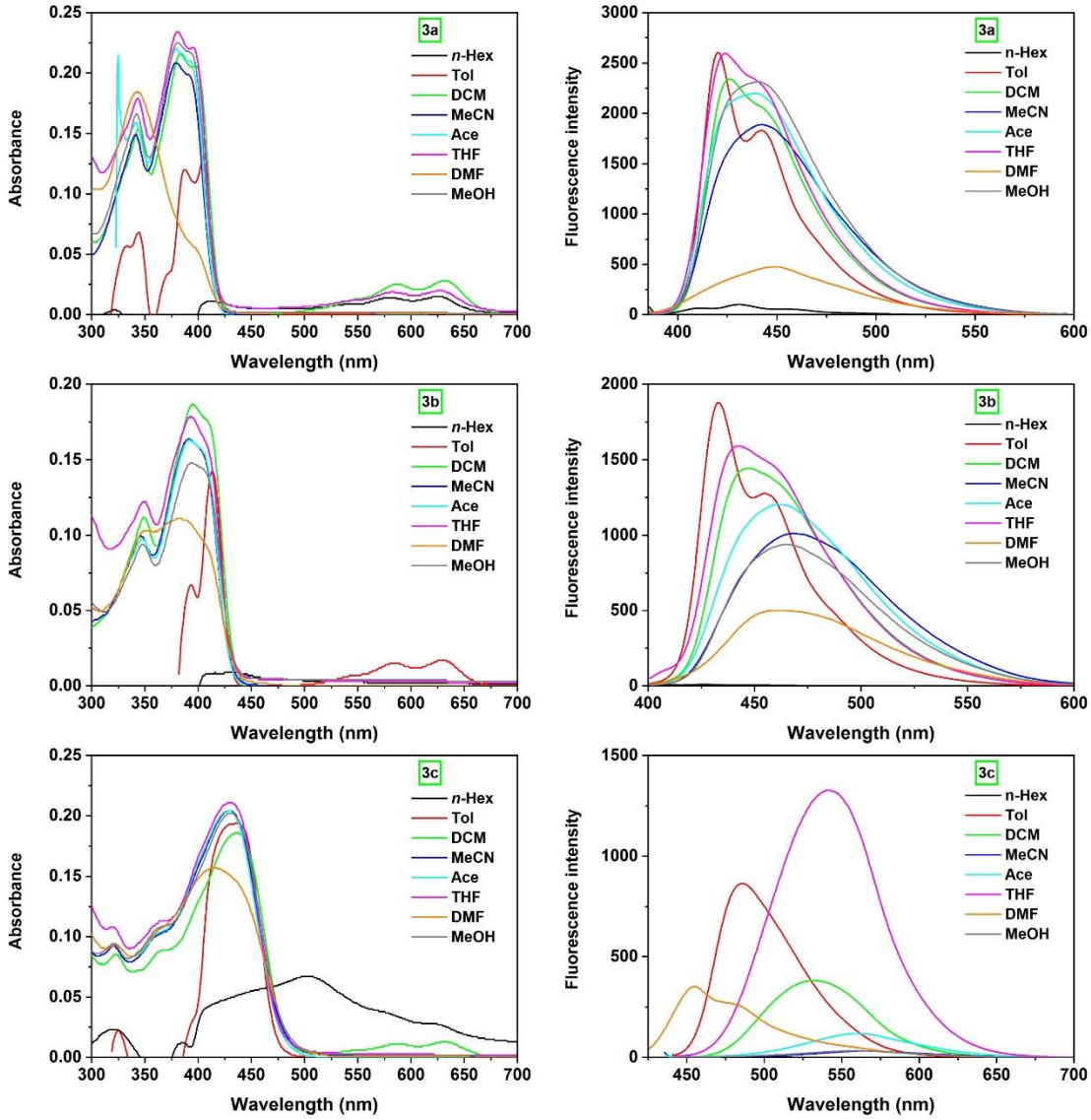


**Fig. S3** Absorption (left) and fluorescence (right) spectra of **3a**–**3c** in various solvents.

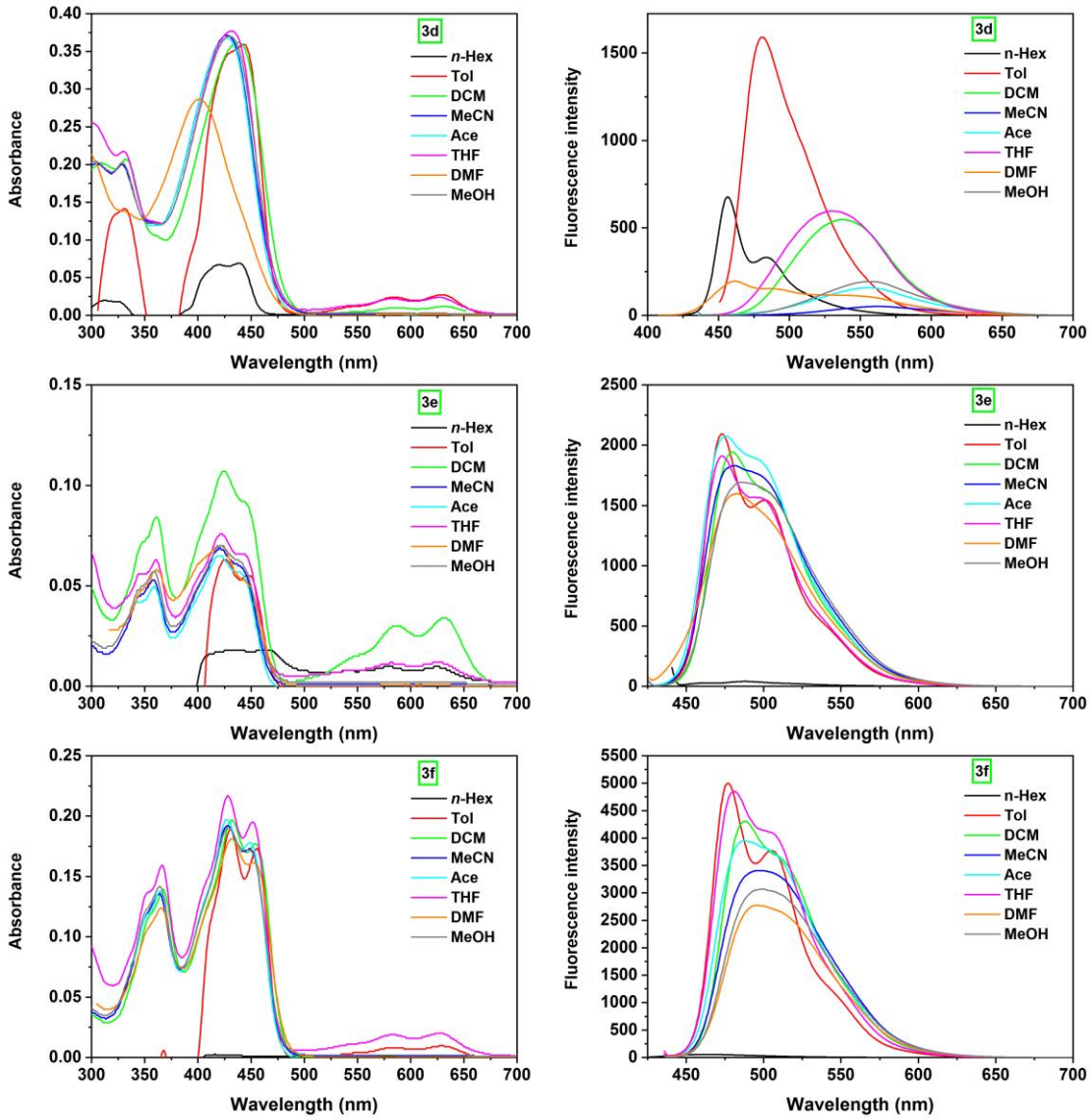


**Fig. S4** Absorption (left) and fluorescence (right) spectra of **3d**–**3f** in various solvents.

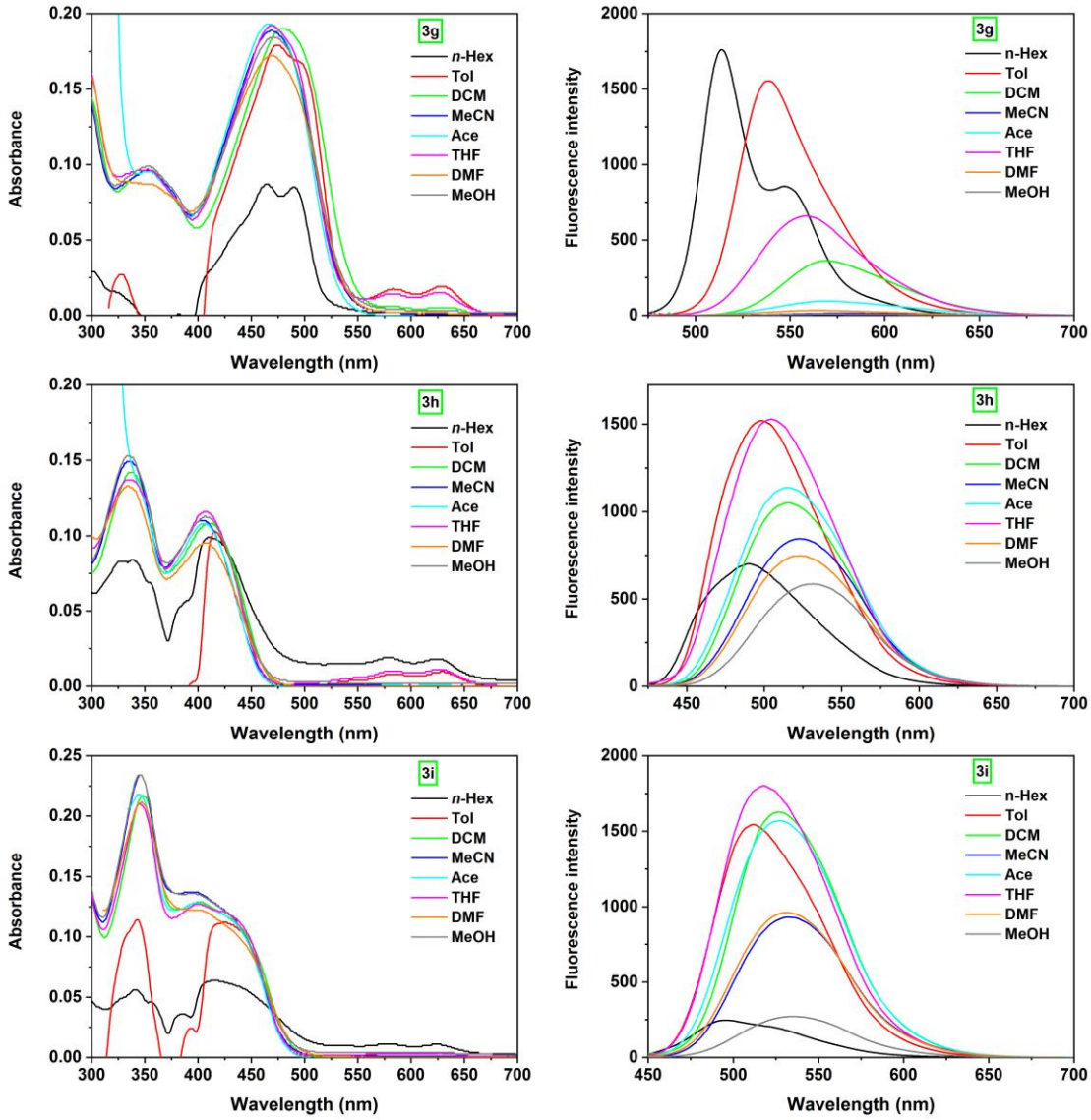


**Fig. S5** Absorption (left) and fluorescence (right) spectra of **3g**–**3i** in various solvents.

**Table S2** Optical data of **3a**–**3i** measured in various solvents at 298 K.

| Compd. | Solvent | $\lambda_{abs}$ /nm ($\varepsilon/\times10^4$ $mol^{-1}$ L $cm^{-1}$) | $\lambda_{em}$/nm | Stokes shift/ $cm^{-1}$ |
|---|---|---|---|---|
| **3a** | *n*-hexane | 625(0.15), 581(0.14), 414(1.10) | 431, 454 | 2128 |
| | toluene | 406(2.62), 387(2.40), 345(1.36) | 420,442 | 3215 |
| | $CH_2Cl_2$ | 635(0.28), 591(0.25), 398(4.12), 383(4.32) | 426 | 2635 |
| | acetonitrile | 381(4.16), 342(2.98) | 442 | 3623 |
| | acetone | 380(4.40) | 439 | 3537 |
| | THF | 630(0.20), 584(0.19),381(4.68), 344(3.58) | 423 | 2606 |
| | DMF | 394(1.16), 343(3.70) | 475 | 4329 |
| | MeOH | 382(4.50), 343(3.32) | 441 | 3502 |
| **3b** | *n*-hexane | 432(1.8) | 448 | 827 |
| | toluene | 633(0.17), 589(0.15), 414(2.84), 394(1.34) | 433,455 | 3403 |
| | $CH_2Cl_2$ | 397(3.72), 351(2.22) | 447 | 2818 |
| | acetonitrile | 392(3.28), 346(2.00) | 468 | 4143 |
| | acetone | 393(3.26), 349(1.94) | 462 | 3800 |
| | THF | 393(3.58), 351(2.44) | 443 | 2872 |
| | DMF | 384(2.22), 353(2.06) | 462 | 4397 |
| | MeOH | 395(2.96), 349(1.88) | 464 | 3764 |
| **3c** | *n*-hexane* | — | — | — |
| | toluene | 438(3.88) | 486 | 2255 |
| | $CH_2Cl_2$ | 634(0.13), 595(0.11), 438(3.72) | 532 | 4034 |
| | acetonitrile | 432(4.08) | 564 | 5418 |
| | acetone | 431(4.08) | 560 | 5345 |
| | THF | 432(4.22) | 542 | 4698 |
| | DMF | 418(3.14) | 454 | 1897 |
| | MeOH | 433(4.04) | 560 | 5237 |
| **3d** | *n*-hexane | 440(1.38), 422(1.34) | 456, 483 | 2023 |
| | toluene | 633(0.27), 589(0.24), 444(7.18), 332(2.82) | 481 | 1732 |
| | $CH_2Cl_2$ | 634(0.12), 595(0.10), 439(7.24), 332(4.14) | 537 | 4157 |
| | acetonitrile | 429(7.42), 329(4.00) | 562 | 5517 |
| | acetone | 428(7.36) | 557 | 5411 |
| | THF | 629(0.24), 588(0.22), 433(7.54), 302(5.10) | 530 | 4227 |
| | DMF | 402(5.74), 297(4.32) | 461, 487, 539 | 6322 |

| | | | | |
|---|---|---|---|---|
| | MeOH | 331(7.40) | 558 | 5281 |
| **3e** | *n*-hexane | 627(0.10), 583(0.10), 464(1.90) | 488 | 1059 |
| | toluene | 450(5.50), 427(6.30) | 473, 502 | 2302 |
| | $CH_2Cl_2$ | 634(0.34), 591(0.30), 426(10.70), 362(8.40) | 480 | 2641 |
| | acetonitrile | 421(6.90), 359(5.30) | 481 | 2963 |
| | acetone | 423(6.50), 359(5.00) | 476 | 2633 |
| | THF | 630(0.12), 583(0.12), 423(7.60), 361(6.30) | 473, 496 | 3480 |
| | DMF | 423(7.00), 362(5.80) | 482 | 2894 |
| | MeOH | 424(7.00), 360(5.79) | 486 | 3009 |
| **3f** | *n*-hexane* | — | — | — |
| | toluene | 631(0.10), 593(0.08), 456(3.46), 431(3.78) | 477, 506 | 2238 |
| | $CH_2Cl_2$ | 455(3.54), 432(3.94), 368(2.78) | 487 | 2614 |
| | acetonitrile | 450(3.44), 429(3.88), 365(2.78) | 499 | 3270 |
| | acetone | 450(3.56), 429(3.92), 365(2.76) | 488 | 2818 |
| | THF | 631(0.20), 586(0.19), 429(4.32), 367(3.18) | 481, 502 | 2520 |
| | DMF | 454(3.22), 433(3.62), 366(2.48) | 497 | 2974 |
| | MeOH | 449(3.44), 430(3.80), 364(2.84) | 499 | 3216 |
| **3g** | *n*-hexane | 491(1.70), 466(1.74) | 514, 547 | 2004 |
| | toluene | 633(0.19), 584(0.18), 477(3.58) | 538 | 2377 |
| | $CH_2Cl_2$ | 641(0.10), 589(0.12), 483(3.80), 358(1.92) | 568 | 3099 |
| | acetonitrile | 470(3.78), 356(1.92) | 578 | 3975 |
| | acetone | 470(3.86), 357(1.90) | 569 | 3702 |
| | THF | 632(0.15), 590(0.14), 471(3.84), 353(1.94) | 558 | 3310 |
| | DMF | 472(3.44), 358(1.74) | 565 | 3487 |
| | MeOH | 471(3.70), 355(1.98) | 572 | 3749 |
| **3h** | *n*-hexane | 630(0.18), 584(0.19), 413(1.98), 340(1.68) | 490 | 3805 |
| | toluene | 631(0.10), 593(0.16), 416(2.06) | 498 | 3958 |
| | $CH_2Cl_2$ | 414(2.16), 339(2.84) | 515 | 4737 |
| | acetonitrile | 407(2.20), 338(2.98) | 524 | 5486 |
| | acetone | 408(2.16) | 515 | 5092 |
| | THF | 633(0.11), 591(0.10), 409(2.32), 339(2.74) | 505 | 4647 |
| | DMF | 410(1.90), 338(2.64) | 524 | 5306 |
| | MeOH | 411(2.24), 336(3.06) | 532 | 5534 |
| **3i** | *n*-hexane | 626(0.11), 587(0.11), 419(1.28), 343(1.12) | 495 | 3664 |

| | | | |
|---|---|---|---|
| toluene | 630(0.08), 588(0.08),427(2.24), 344(2.28) | 512 | 3888 |
| $CH_2Cl_2$ | 404(2.58), 349(4.34) | 527 | 5777 |
| acetonitrile | 400(2.74), 347(4.68) | 533 | 6238 |
| acetone | 402(2.56), 346(4.36) | 528 | 5936 |
| THF | 408(2.54), 346(4.20) | 518 | 5204 |
| DMF | 404(2.44), 347(4.24) | 532 | 5955 |
| MeOH | 398(2.72), 347(4.68) | 537 | 6503 |

* poor solubility.

**Fig. S6** Photographs of **3a**–**3i** taken under UV light (365 nm) in DCM.

**Fig. S7** Photographs of **3a**–**3i** taken under UV light (365 nm) in THF.

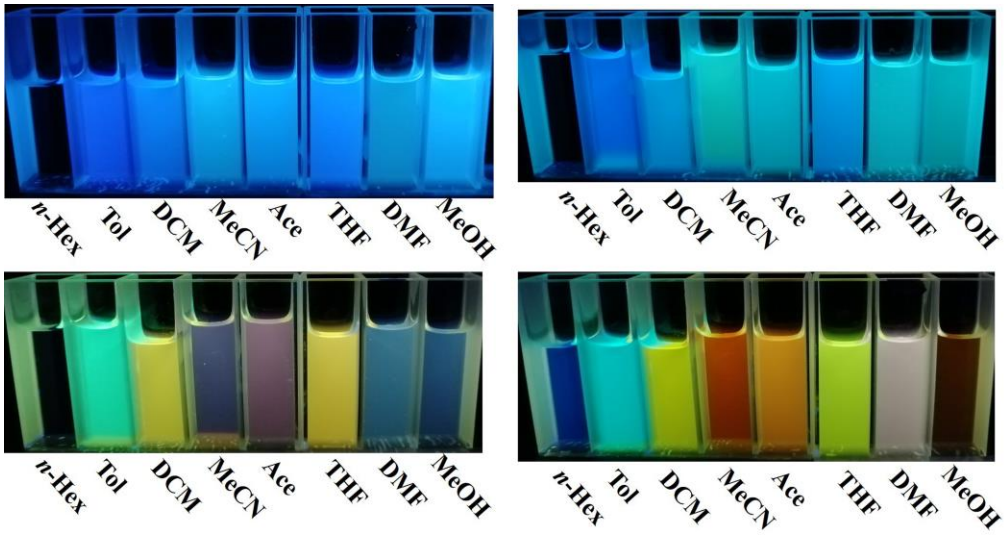


**Fig. S8** Photographs of **3a**–**3d** taken under UV light (365 nm) in different solvents.

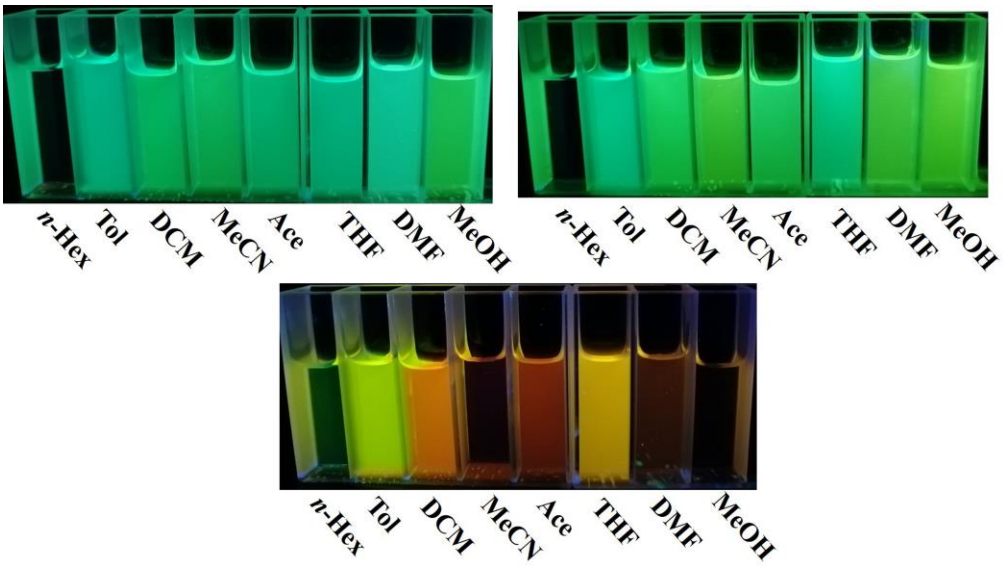


**Fig. S9** Photographs of **3e**–**3g** taken under UV light (365 nm) in different solvents.

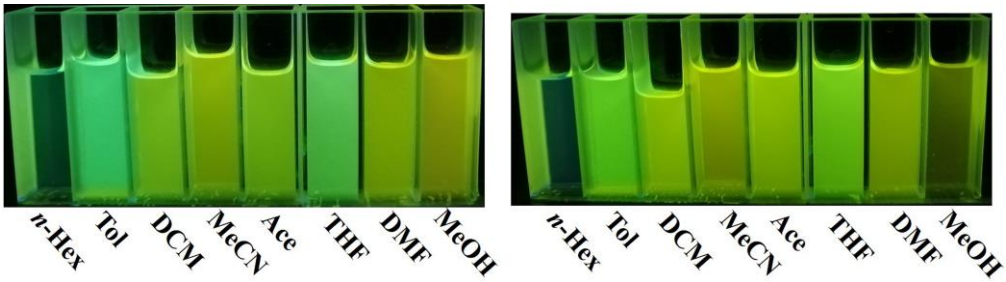


**Fig. S10** Photographs of **3h**–**3i** taken under UV light (365 nm) in different solvents.

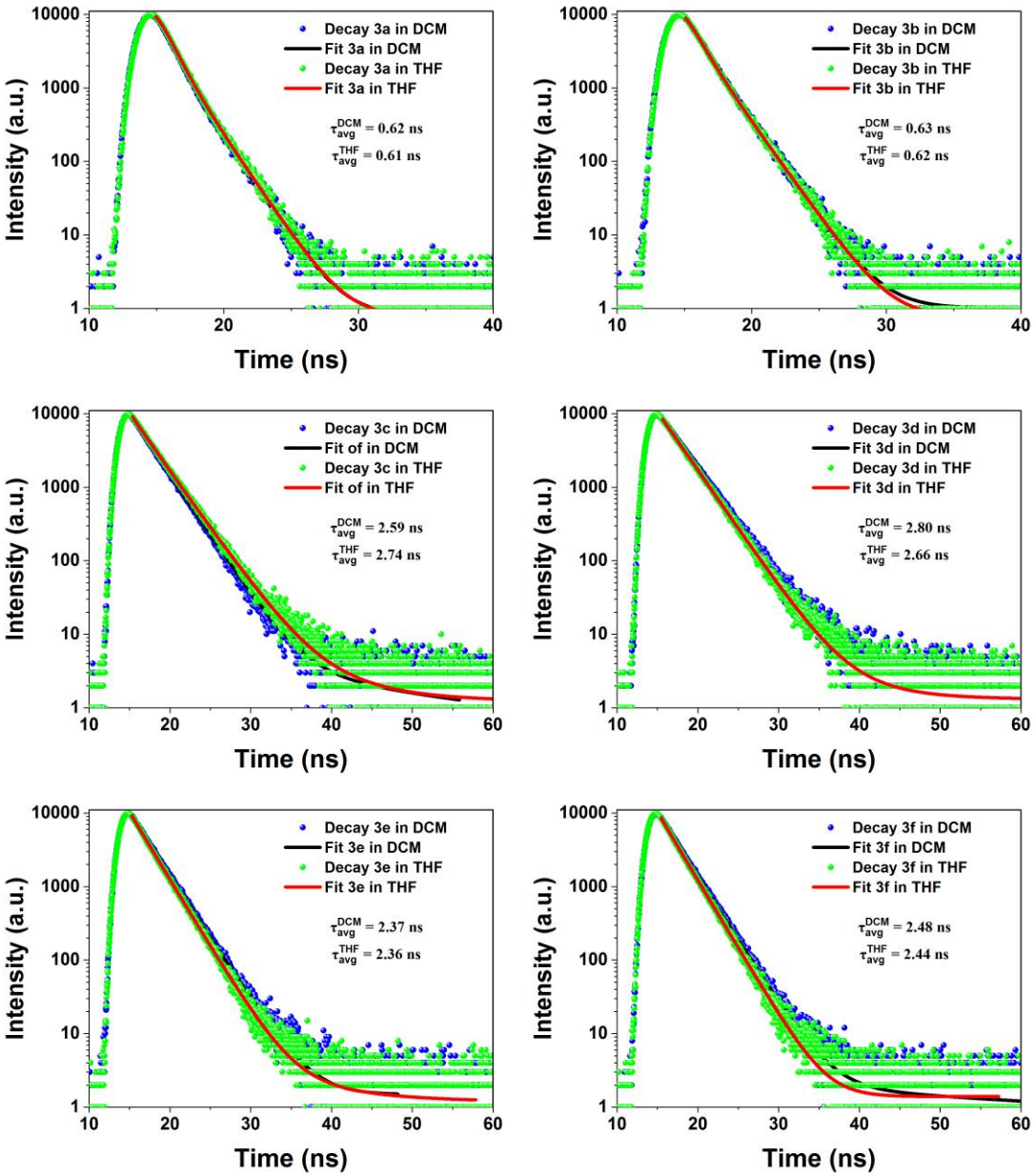


**Fig. S11** Photoluminescence decay curves of compounds **3a**–**3f**, respectively, measured with TCSPC in DCM and THF under air at 298 K.

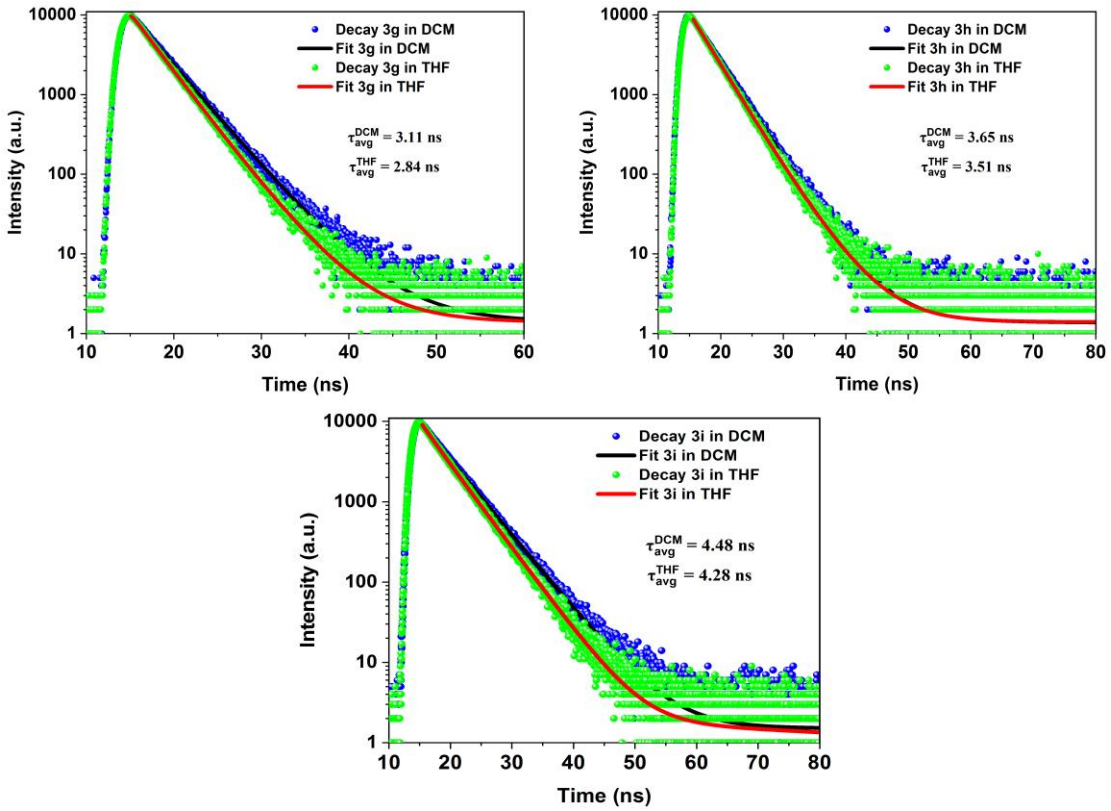


**Fig. S12** Photoluminescence decay curves of compounds **3g**–**3i**, respectively, measured with TCSPC in DCM and THF under air at 298 K.

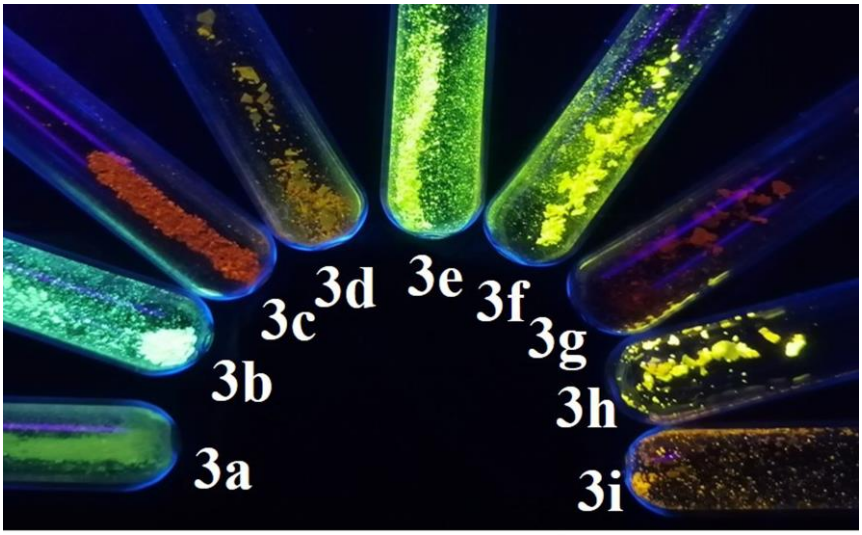


**Fig. S13** Photographs of **3a**–**3i** in solid state taken under UV light (365 nm).

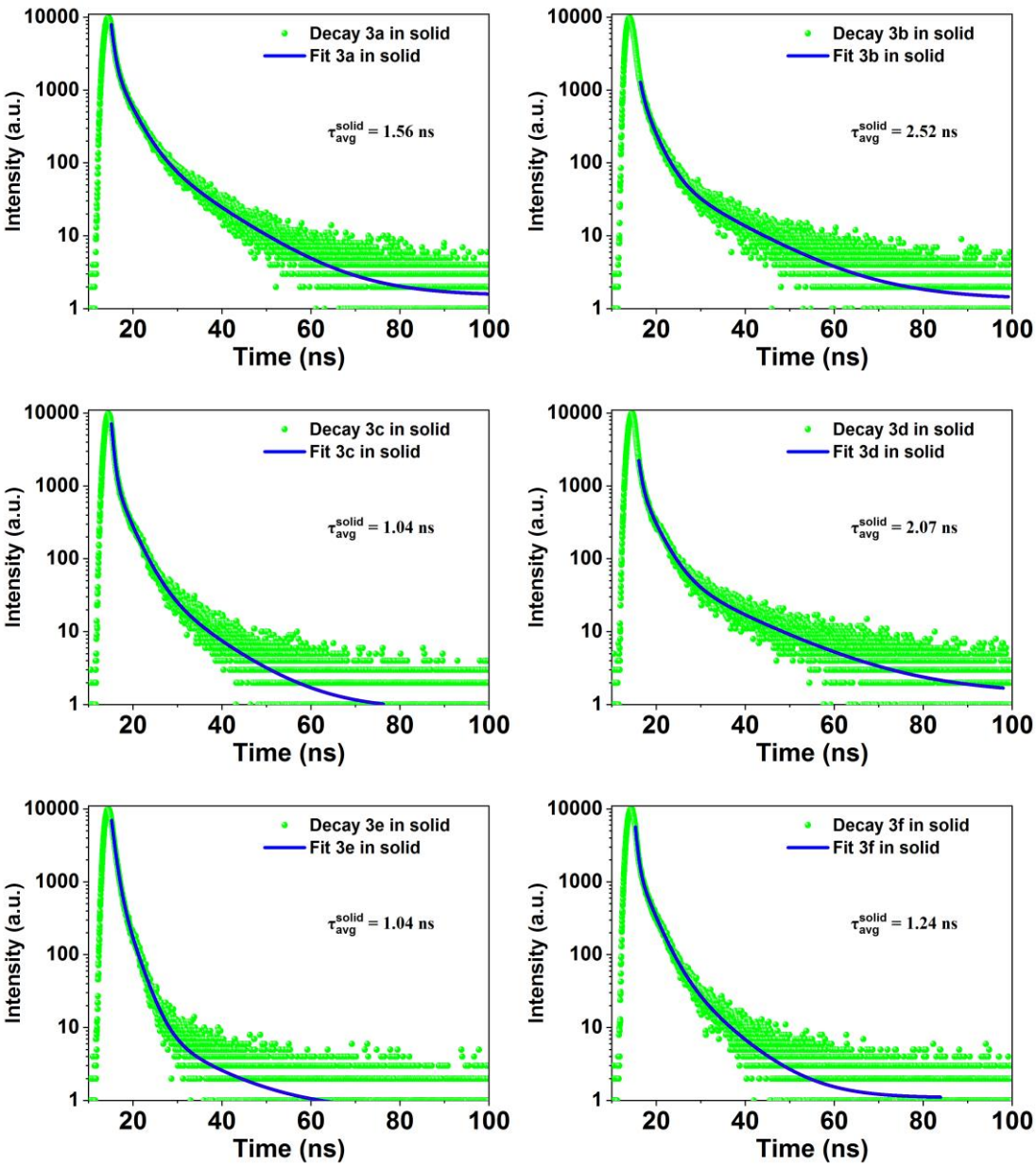


**Fig. S14** Photoluminescence decay curves of the solid compounds **3a**–**3f**, respectively, measured with TCSPC under air at 298 K.

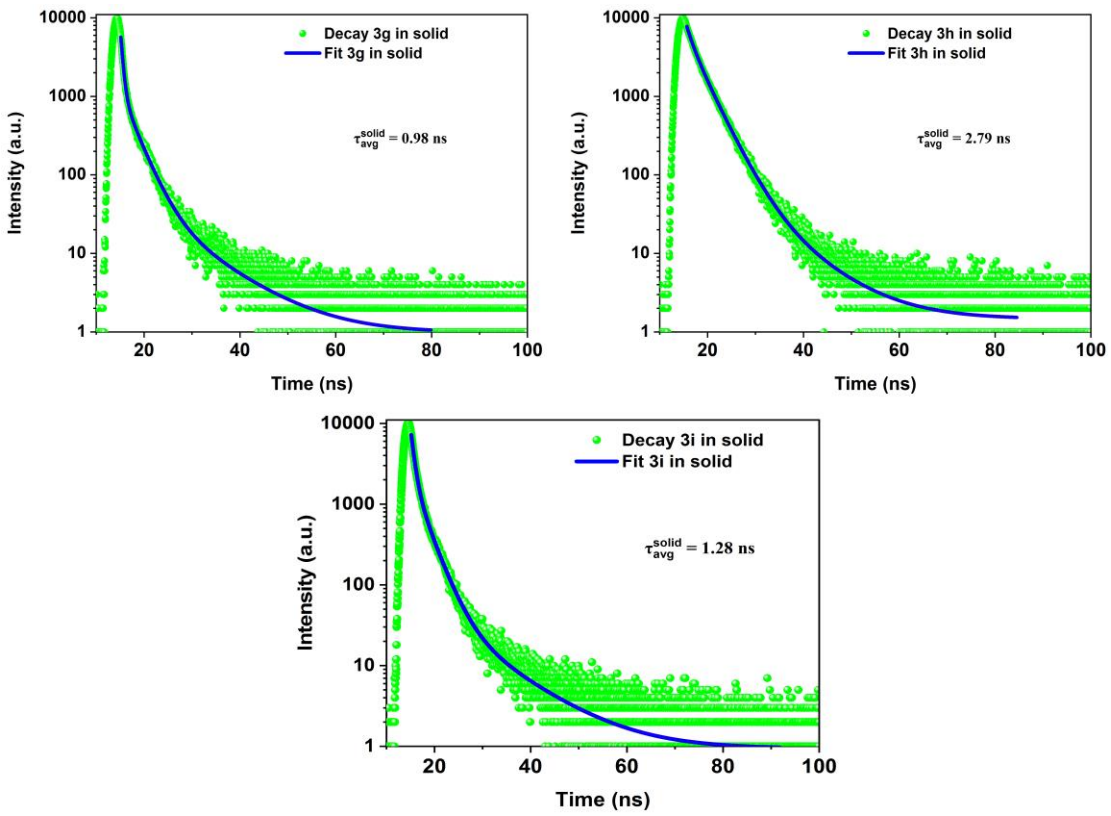


**Fig. S15** Photoluminescence decay curves of the solid compounds **3g**–**3i**, respectively, measured with TCSPC under air at 298 K.

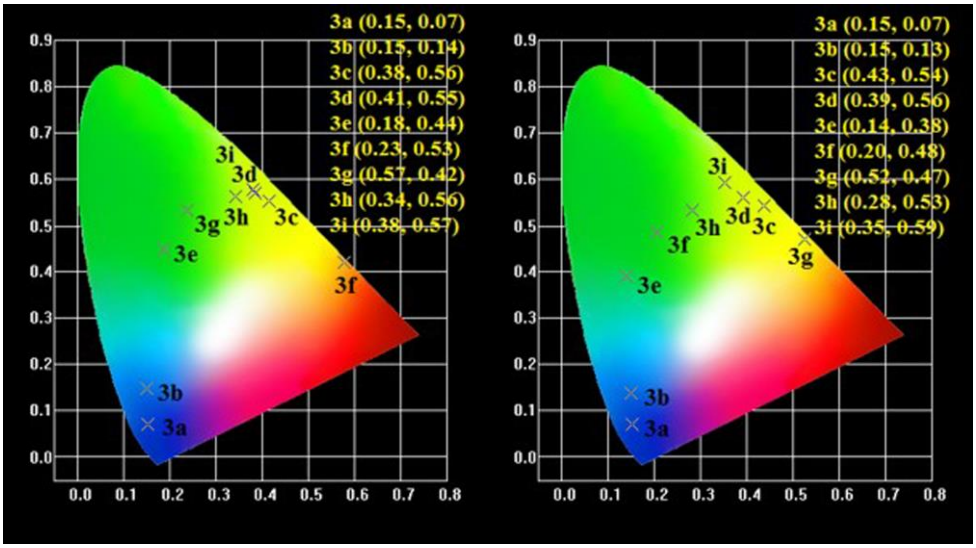


**Fig. S16** CIE−1931 coordinates diagram of **3a**–**3i** in DCM (left) and THF (right).

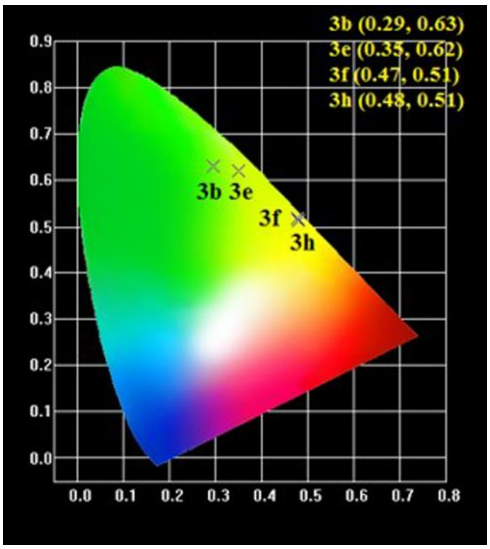


**Fig. S17** CIE−1931 coordinates diagram of **3b**, **3e**, **3f** and **3h** in solid state. The signal of **3a**, **3c**, **3d**, **3g** and **3i** are too weak to be accurately determined.

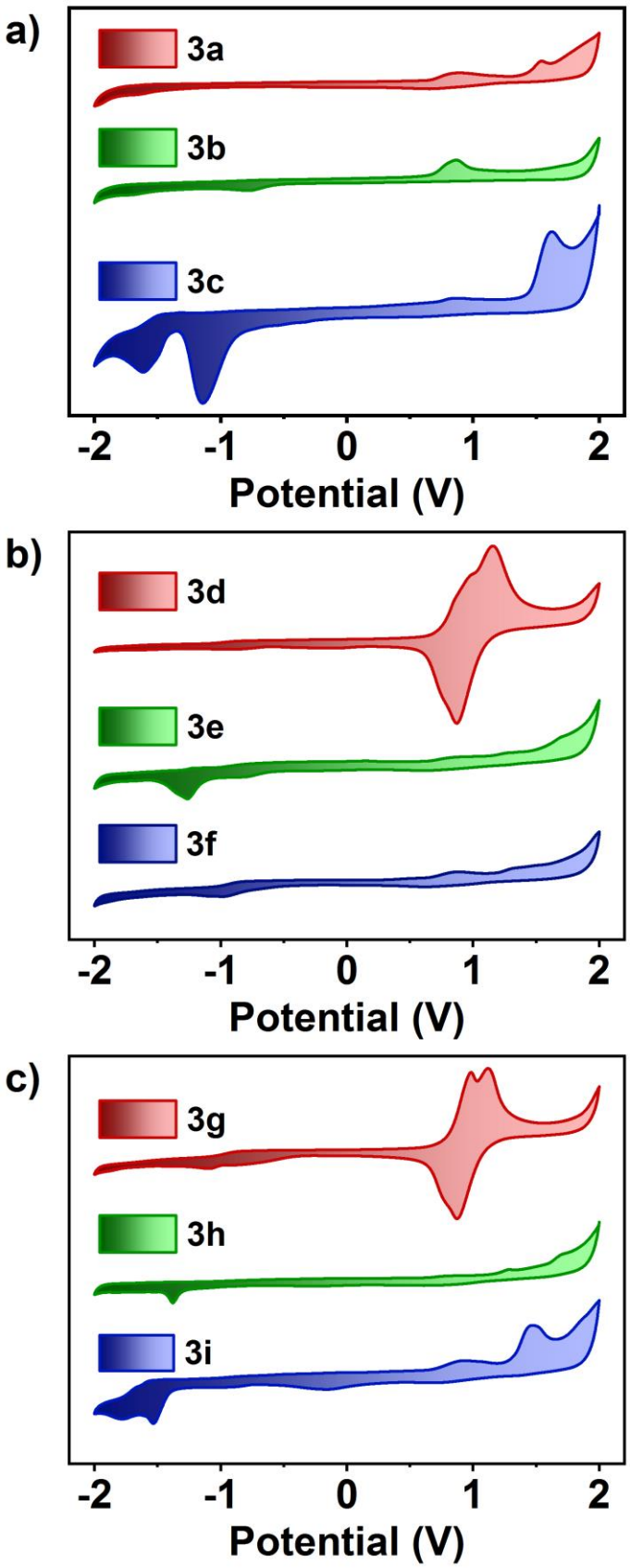


**Fig. S18** Cyclic voltammetry curves of **3a**–**3i** with 0.1 M *n*-$Bu_4NPF_6$ in DCM solution at a scan rate of 100 mV $s^{-1}$.

**Table S3**. Electrochemical potentials and energy levels of compounds **3a**–**3i**.

| Compd. | $\lambda_{abs}$ /nm[a] | $\lambda_{em}$/nm[a] | $E_{ox}$ /$E_{red}$[b] (V) | $E_{HOMO}$[c] (eV) | $E_{LUMO}$[d] (eV) | $E_g$[e] (eV) | $E_g$[f] (eV) |
|---|---|---|---|---|---|---|---|
| **3a** | 406, 398 | 430, 458 | 1.64 / –1.18<br>1.41 / —<br>0.64 / — | –6.38 | –3.43 | 2.95 | 3.22 |
| **3b** | 395, 349 | 447 | 1.62 / –1.35<br>0.65 / –0.56 | –6.36 | –3.53 | 2.83 | 3.15 |
| **3c** | 436 | 531 | 1.44 / –0.82<br>0.66 / –0.43 | –6.18 | –3.64 | 2.54 | 2.85 |
| **3d** | 443 | 537 | 1.54 / –0.64<br>0.70 / — | –6.28 | –3.74 | 2.54 | 2.74 |
| **3e** | 425 | 479 | 1.58 / –1.10<br>0.66 / –0.59 | –6.32 | –3.70 | 2.62 | 3.01 |
| **3f** | 454,<br>432, 367 | 487 | 1.58 / –0.50<br>0.66 / — | –6.32 | –3.76 | 2.56 | 2.95 |
| **3g** | 480 | 568 | 1.53 / –0.99<br>0.77 / –0.43 | –6.27 | –4.05 | 2.22 | 2.50 |
| **3h** | 412,337 | 515 | 1.41 / –1.29<br>1.16 / —<br>0.64 / — | –6.15 | –3.49 | 2.66 | 3.50 |
| **3i** | 402, 348 | 526 | 1.28 / –1.38<br>0.66 / –0.74 | –6.02 | –3.48 | 2.54 | 2.73 |

[a] $1.0\times10^{-3}$ M in DCM.

[b] Onset voltages in CV curves.

[c] $E_{HOMO} = -E_{ox} - 4.74$ eV.

[d] $E_{LUMO} = E_{HOMO} + E_g$.

[e] $E_g$ estimated from the UV–vis absorption spectra.

[f] $E_g$ is by DFT theoretical calculations.

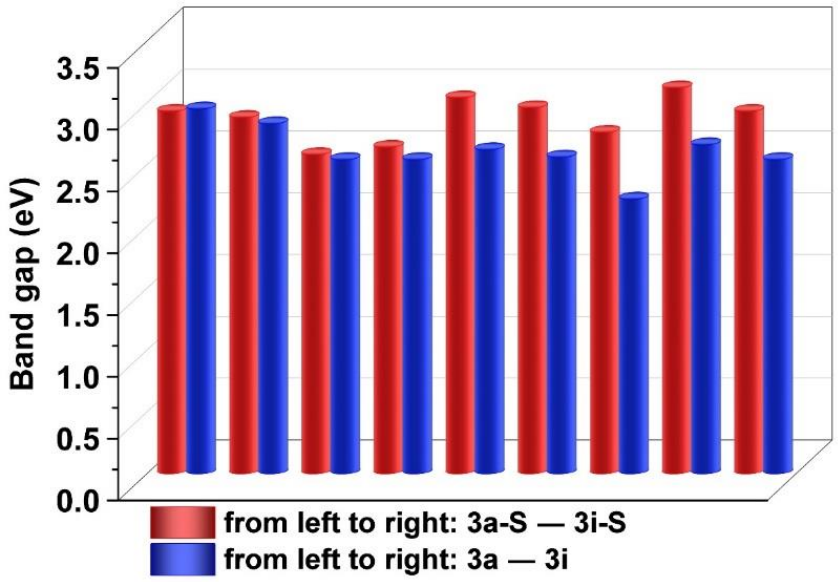


**Fig. S19** The electrochemical gaps of new luminogens **3a**–**3i** and sulfuric precursors **3a-S**–**3i-S**. The data of **3a-S**–**3i-S** are obtained from the recently literatures.[S1, S2]

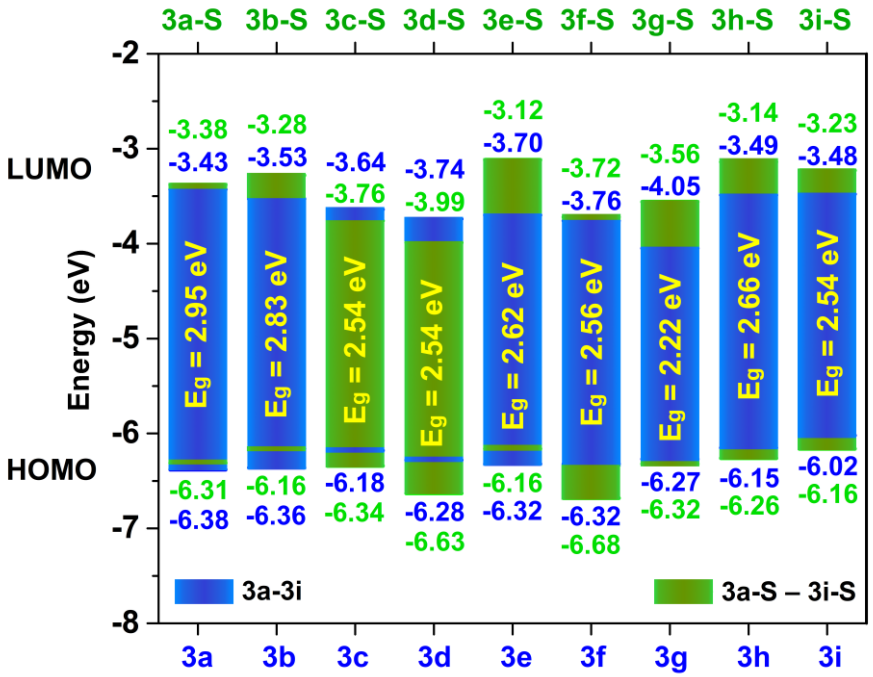


**Fig. S20** Experimental energy level diagram of the frontier orbitals of **3a**–**3i** in comparison with the sulfuric precursors **3a-S**–**3i-S**. The data of **3a-S**–**3i-S** are obtained from the recently literatures.[S1, S2]

## 5. TD–DFT calculation data

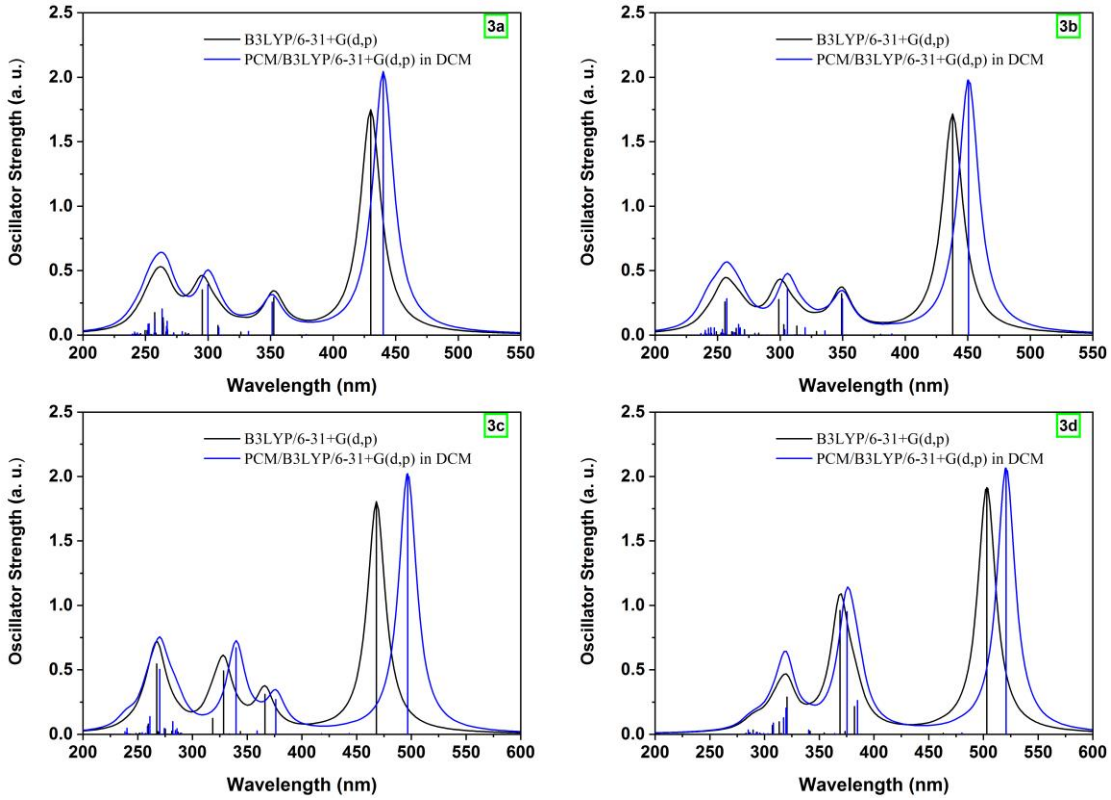


**Fig. S21** Predicted UV–vis spectra of **3a**–**3d** based on TD–DFT calculation.

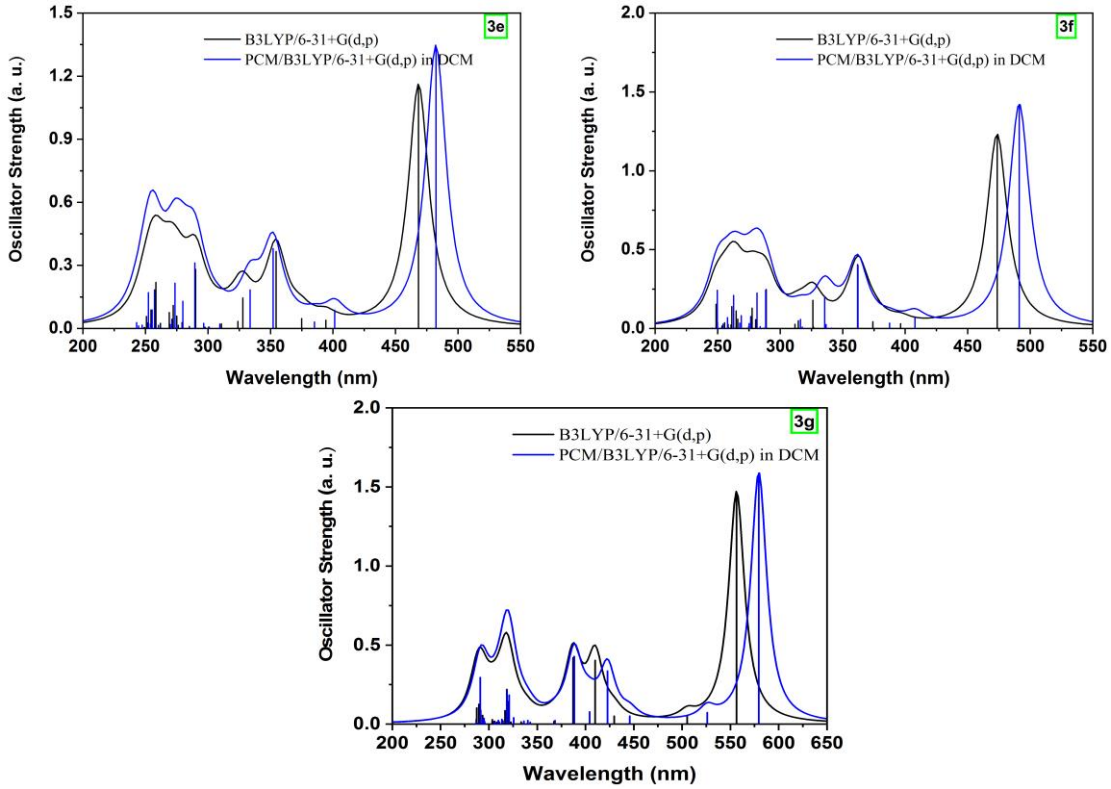


**Fig. S22** Predicted UV–vis spectra of **3e**–**3g** based on TD–DFT calculation.

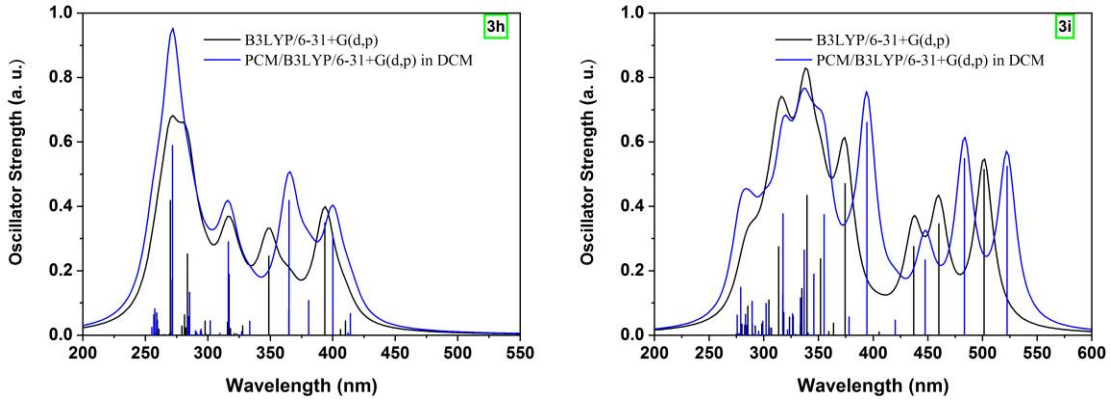


**Fig. S23** Predicted UV–vis spectra of **3h**–**3i** based on TD–DFT calculation.

**Table S4**. Absorption maxima, main orbital transitions, oscillator strengths (*f*) of **3a** to **3i** calculated by the TD–DFT B3LYP/6–31+G(d,p) level in gas state.

| Compd. | Electronic transitions | Energy (eV) | $\lambda_{ab}$ / nm | $^{a}\lambda_{ab}$ / nm and error ratio (%) | Main orbital transition | *f* |
|---|---|---|---|---|---|---|
| **3a** | $S_0 \rightarrow S_1$ | 2.88 | 430.0 | 406 (5.9%) 381 (12.8%) | HOMO → LUMO (98.3%) | 1.74 |
| | $S_0 \rightarrow S_3$ | 3.51 | 352.6 | | HOMO → LUMO+1 (93.9%) | 0.29 |
| | $S_0 \rightarrow S_7$ | 4.19 | 295.3 | | HOMO–1 → LUMO+2 (92.4%) | 0.35 |
| | $S_0 \rightarrow S_{17}$ | 4.69 | 264.1 | | HOMO → LUMO+6 (55.1%) | 0.13 |
| | $S_0 \rightarrow S_{20}$ | 4.82 | 257.2 | | HOMO–1 → LUMO+3 (81.9%) | 0.17 |
| **3b** | $S_0 \rightarrow S_1$ | 2.83 | 437.9 | 395 (10.6%) 393 (11.2%) | HOMO → LUMO (98.3%) | 1.71 |
| | $S_0 \rightarrow S_3$ | 3.55 | 349.2 | | HOMO → LUMO+1 (93.9%) | 0.32 |
| | $S_0 \rightarrow S_9$ | 4.15 | 298.9 | | HOMO–1 → LUMO+2 (84.2%) | 0.27 |
| | $S_0 \rightarrow S_{19}$ | 4.84 | 255.9 | | HOMO–1 → LUMO+3 (40.8%) | 0.26 |
| **3c** | $S_0 \rightarrow S_1$ | 2.65 | 468.1 | 436 (7.3%) 430 (8.8%) | HOMO → LUMO (98.8%) | 1.79 |
| | $S_0 \rightarrow S_3$ | 3.38 | 366.2 | | HOMO → LUMO+1 (95.6%) | 0.31 |
| | $S_0 \rightarrow S_6$ | 3.77 | 328.5 | | HOMO–2 → LUMO (75.2%) | 0.49 |
| | $S_0 \rightarrow S_7$ | 3.89 | 318.5 | | HOMO–1 → LUMO+2 (75.3%) | 0.12 |
| | $S_0 \rightarrow S_{19}$ | 4.64 | 267.2 | | HOMO → LUMO+6 (63.4%) | 0.54 |
| **3d** | $S_0 \rightarrow S_1$ | 2.46 | 503.1 | 443 (13.5%) 432 (16.4%) | HOMO → LUMO (97.5%) | 1.91 |
| | $S_0 \rightarrow S_3$ | 3.24 | 382.3 | | HOMO → LUMO+1 (94.3%) | 0.21 |
| | $S_0 \rightarrow S_5$ | 3.36 | 368.9 | | HOMO–2 → LUMO (67.7%) | 0.96 |
| | $S_0 \rightarrow S_{11}$ | 3.87 | 320.5 | | HOMO → LUMO+7 (59.2%) | 0.29 |
| **3e** | $S_0 \rightarrow S_1$ | 2.65 | 468.4 | 425 (10.1%) 442 (5.8%) | HOMO → LUMO (97.7%) | 1.15 |
| | $S_0 \rightarrow S_4$ | 3.49 | 354.4 | | HOMO → LUMO+2 (90.4%) | 0.36 |
| | $S_0 \rightarrow S_5$ | 3.78 | 327.8 | | HOMO–1 → LUMO+1 (79.6%) | 0.14 |
| | $S_0 \rightarrow S_{11}$ | 4.27 | 290.1 | | HOMO–5 → LUMO (81.9%) | 0.28 |
| | $S_0 \rightarrow S_{17}$ | 4.55 | 272.1 | | HOMO–7 → LUMO (29.1%) | 0.11 |
| | $S_0 \rightarrow S_{22}$ | 4.79 | 258.3 | | HOMO–1 → LUMO+3 (46.4%) | 0.22 |
| **3f** | $S_0 \rightarrow S_1$ | 2.62 | 473.5 | 454 (4.2%) 428 (10.5%) | HOMO → LUMO (97.7%) | 1.23 |
| | $S_0 \rightarrow S_4$ | 3.42 | 362.2 | | HOMO → LUMO+2 (91.9%) | 0.40 |
| | $S_0 \rightarrow S_7$ | 3.80 | 326.1 | | HOMO–1 → LUMO+1 (82.4%) | 0.18 |
| | $S_0 \rightarrow S_{11}$ | 4.29 | 288.8 | | HOMO–5 → LUMO (79.4%) | 0.25 |
| | $S_0 \rightarrow S_{15}$ | 4.46 | 277.5 | | HOMO–6 → LUMO (32.3%) | 0.13 |
| | $S_0 \rightarrow S_{21}$ | 4.68 | 264.7 | | HOMO–1 → LUMO+3 (54.4%) | 0.11 |
| | $S_0 \rightarrow S_{22}$ | 4.74 | 261.3 | | HOMO–2 → LUMO+2 (43.8%) | 0.14 |
| **3g** | $S_0 \rightarrow S_1$ | 2.23 | 556.4 | 480 (15.8%) 469 (18.5%) | HOMO → LUMO (97.2%) | 1.46 |
| | $S_0 \rightarrow S_4$ | 3.02 | 410.0 | | HOMO–1 → LUMO+1 (84.0%) | 0.40 |
| | $S_0 \rightarrow S_6$ | 3.20 | 387.1 | | HOMO → LUMO+2 (73.5%) | 0.42 |
| | $S_0 \rightarrow S_{13}$ | 3.88 | 319.3 | | HOMO → LUMO+8 (26.8%) | 0.14 |
| | $S_0 \rightarrow S_{14}$ | 3.89 | 318.6 | | HOMO → LUMO+7(52.9%) | 0.22 |
| | $S_0 \rightarrow S_{28}$ | 4.28 | 289.5 | | HOMO–12 → LUMO (28.4%) | 0.12 |
| | $S_0 \rightarrow S_{29}$ | 4.31 | 287.4 | | HOMO → LUMO+13 (39.7%) | 0.10 |

| | | | | | | |
|---|---|---|---|---|---|---|
| **3h** | $S_0 \rightarrow S_1$ | 3.02 | 410.2 | | HOMO → LUMO (84.9%) | 0.04 |
| | $S_0 \rightarrow S_3$ | 3.15 | 393.7 | | HOMO–2 → LUMO (83.4%) | 0.35 |
| | $S_0 \rightarrow S_5$ | 3.55 | 348.8 | 412 (0.5%) | HOMO–4 → LUMO (95.0%) | 0.24 |
| | $S_0 \rightarrow S_{10}$ | 3.91 | 316.9 | 407 (0.7%) | HOMO → LUMO+2 (24.1%) | 0.18 |
| | $S_0 \rightarrow S_{18}$ | 4.37 | 283.7 | | HOMO–8 → LUMO (56.0%) | 0.25 |
| | $S_0 \rightarrow S_{23}$ | 4.59 | 269.9 | | HOMO–4 → LUMO+2 (66.1%) | 0.42 |
| **3i** | $S_0 \rightarrow S_1$ | 2.47 | 501.4 | | HOMO → LUMO (97.6%) | 0.51 |
| | $S_0 \rightarrow S_2$ | 2.69 | 460.1 | | HOMO–1 → LUMO (97.9%) | 0.34 |
| | $S_0 \rightarrow S_3$ | 2.83 | 437.1 | | HOMO → LUMO+1 (97.6%) | 0.27 |
| | $S_0 \rightarrow S_5$ | 3.31 | 374.4 | | HOMO–2 → LUMO (91.6%) | 0.47 |
| | $S_0 \rightarrow S_8$ | 3.52 | 351.8 | 402 (24.6%) | HOMO → LUMO+2 (76.4%) | 0.24 |
| | $S_0 \rightarrow S_9$ | 3.65 | 339.5 | 400 (25.2%) | HOMO → LUMO+3 (89.4%) | 0.43 |
| | $S_0 \rightarrow S_{10}$ | 3.70 | 334.8 | | HOMO–2 → LUMO+1 (44.1%) | 0.14 |
| | $S_0 \rightarrow S_{15}$ | 3.91 | 317.3 | | HOMO–6 → LUMO (68.9%) | 0.12 |
| | $S_0 \rightarrow S_{16}$ | 3.95 | 313.6 | | HOMO–1 → LUMO+3 (67.5%) | 0.27 |
| | $S_0 \rightarrow S_{18}$ | 4.07 | 304.6 | | HOMO–7 → LUMO (72.3%) | 0.11 |

[a] Experimental values measured in dichloromethane and THF.

**Table S5**. Absorption maxima, main orbital transitions, oscillator strengths (*f*) of **3a** to **3i** calculated by the TD–DFT B3LYP/6–31+G(d,p) level in gas and $CH_2Cl_2$ solution.

| Compd. | Electronic transitions | Energy (eV) | $\lambda_{ab}$ / nm | [c] $\lambda_{ab}$ / nm and error ratio (%) | Main orbital transition | *f* |
|---|---|---|---|---|---|---|
| **3a** | [a] $S_0 \rightarrow S_1$ | 2.88 | 430.0 | 406 (5.9%) | HOMO → LUMO (98.3%) | 1.74 |
| | [b] $S_0 \rightarrow S_1$ | 2.82 | 440.1 | 381 (12.8%) | HOMO → LUMO (98.4%) | 2.04 |
| **3b** | [a] $S_0 \rightarrow S_1$ | 2.83 | 437.9 | 395 (10.6%) | HOMO → LUMO (98.3%) | 1.71 |
| | [b] $S_0 \rightarrow S_1$ | 2.75 | 450.6 | 393 (11.2%) | HOMO → LUMO (98.3%) | 1.98 |
| **3c** | [a] $S_0 \rightarrow S_1$ | 2.65 | 468.1 | 436 (7.3%) | HOMO → LUMO (98.8%) | 1.79 |
| | [b] $S_0 \rightarrow S_1$ | 2.49 | 496.6 | 430 (8.8%) | HOMO → LUMO (98.6%) | 2.02 |
| **3d** | [a] $S_0 \rightarrow S_1$ | 2.46 | 503.1 | 443 (13.5%) | HOMO → LUMO (97.5%) | 1.91 |
| | [b] $S_0 \rightarrow S_1$ | 2.38 | 520.7 | 432 (16.4%) | HOMO → LUMO (96.8%) | 2.06 |
| **3e** | [a] $S_0 \rightarrow S_1$ | 2.65 | 468.4 | 425 (10.1%) | HOMO → LUMO (97.7%) | 1.15 |
| | [b] $S_0 \rightarrow S_1$ | 2.57 | 482.3 | 442 (5.8%) | HOMO → LUMO (97.9%) | 1.34 |
| **3f** | [a] $S_0 \rightarrow S_1$ | 2.62 | 473.5 | 454 (4.2%) | HOMO → LUMO (97.7%) | 1.23 |
| | [b] $S_0 \rightarrow S_1$ | 2.52 | 491.1 | 428 (10.5%) | HOMO → LUMO (97.9%) | 1.42 |
| **3g** | [a] $S_0 \rightarrow S_1$ | 2.23 | 556.4 | 480 (15.8%) | HOMO → LUMO (97.2%) | 1.46 |
| | [b] $S_0 \rightarrow S_1$ | 2.14 | 579.4 | 469 (18.5%) | HOMO → LUMO (96.4%) | 1.58 |
| **3h** | [a] $S_0 \rightarrow S_1$ | 3.02 | 410.2 | 412 (0.5%) | HOMO → LUMO (84.9%) | 0.04 |
| | [b] $S_0 \rightarrow S_1$ | 2.99 | 414.1 | 407 (0.7%) | HOMO → LUMO (85.8%) | 0.07 |
| **3i** | [a] $S_0 \rightarrow S_1$ | 2.47 | 501.4 | 402 (24.6%) | HOMO → LUMO (97.6%) | 0.51 |
| | [b] $S_0 \rightarrow S_1$ | 2.37 | 522.5 | 400 (25.2%) | HOMO → LUMO (96.8%) | 0.52 |

[a] Calculated by the TD–DFT B3LYP/6–31+G(d,p) level in gas.

[b] Calculated by the TD–DFT B3LYP/6–31+G(d,p) level in DCM solution.

[c] Experimental values measured in dichloromethane and THF.

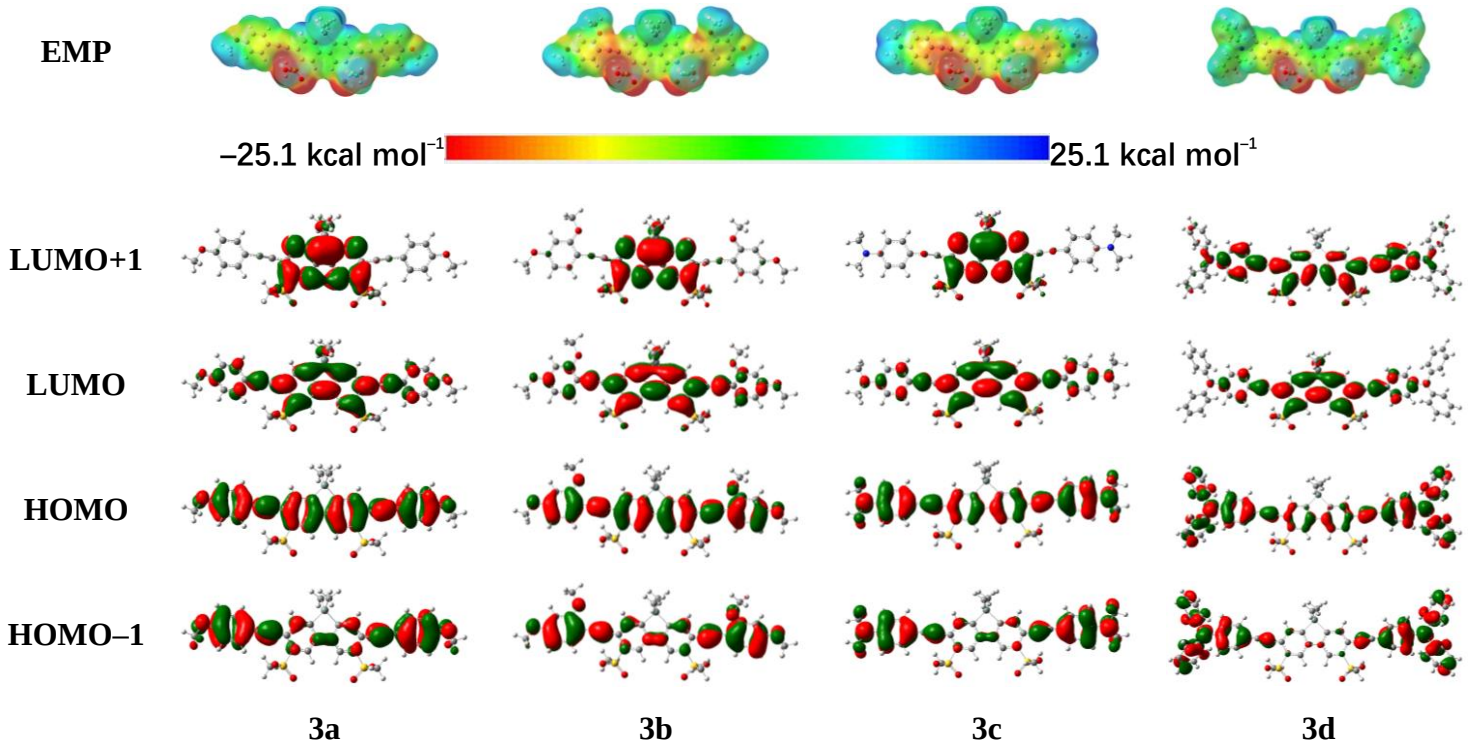


**Fig. S24** Frontier molecular orbitals and electrostatic potential maps of **3a**–**3d**.

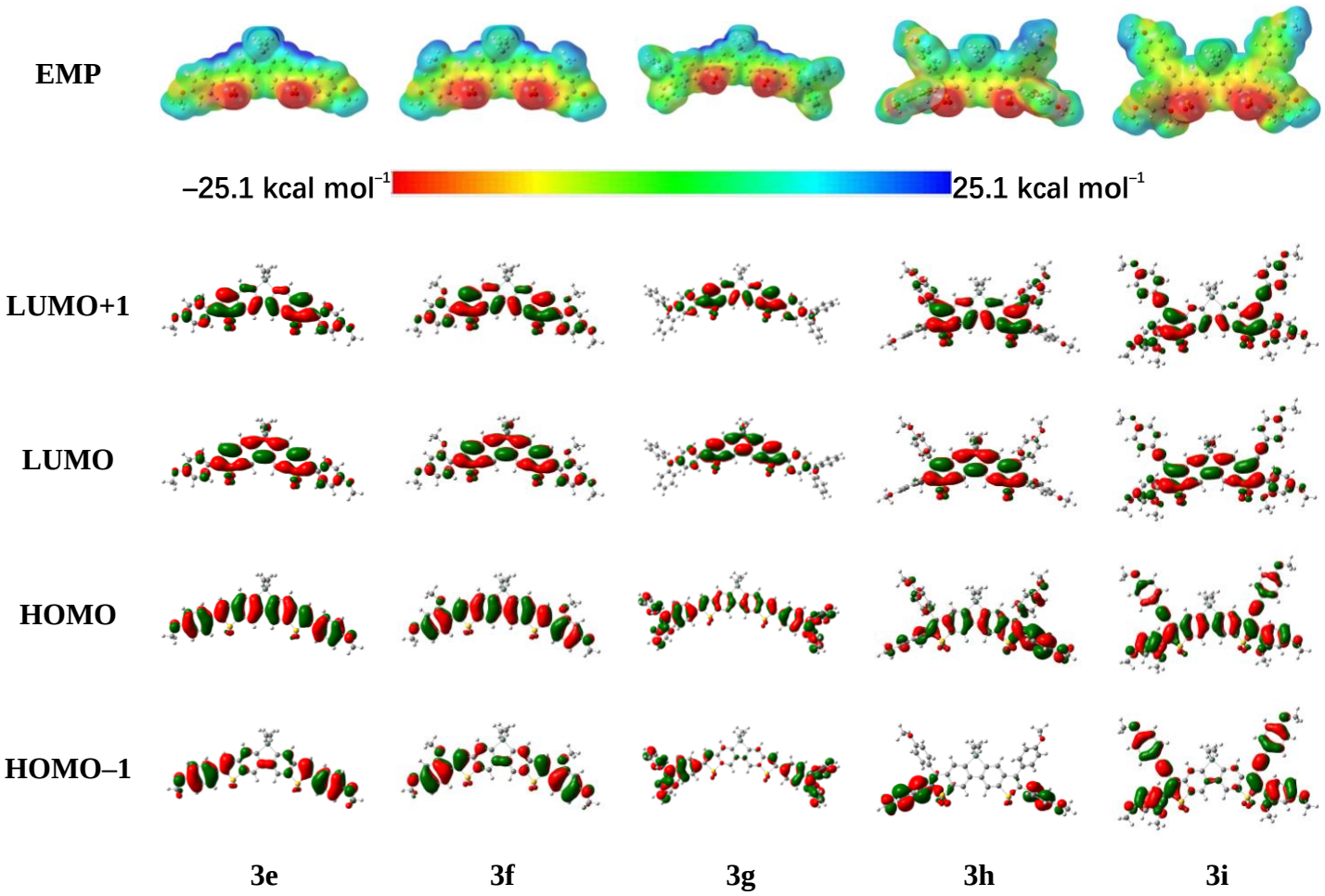


**Fig. S25** Frontier molecular orbitals and electrostatic potential maps of **3c**–**3i**.

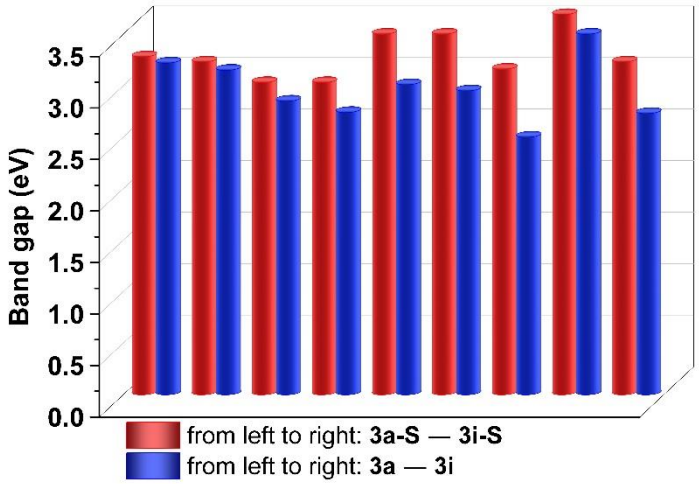


**Fig. S26** The calculated band gaps of sulfone-based luminogens **3a**–**3i** and sulfide-based luminogens **3a-S**–**3i-S**. The data of **3a-S**–**3i-S** are obtained from the recent literatures.[S1, S2]

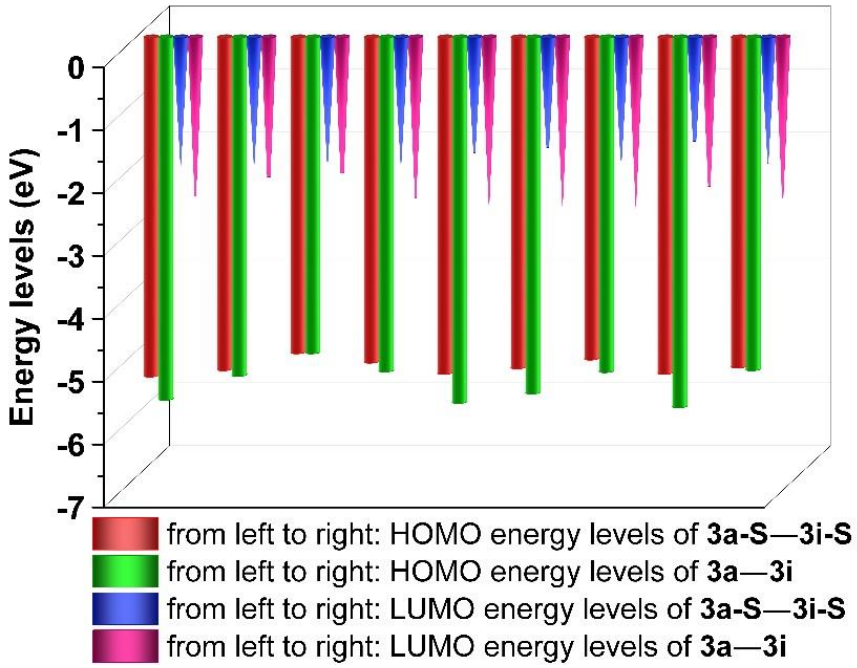


**Fig. S27** The calculated HOMO and LUMO energy levels of **3a**–**3i** and sulfuric ones **3a-S**–**3i-S**. The data of **3a-S**–**3i-S** are obtained from the recent literatures.[S1, S2]

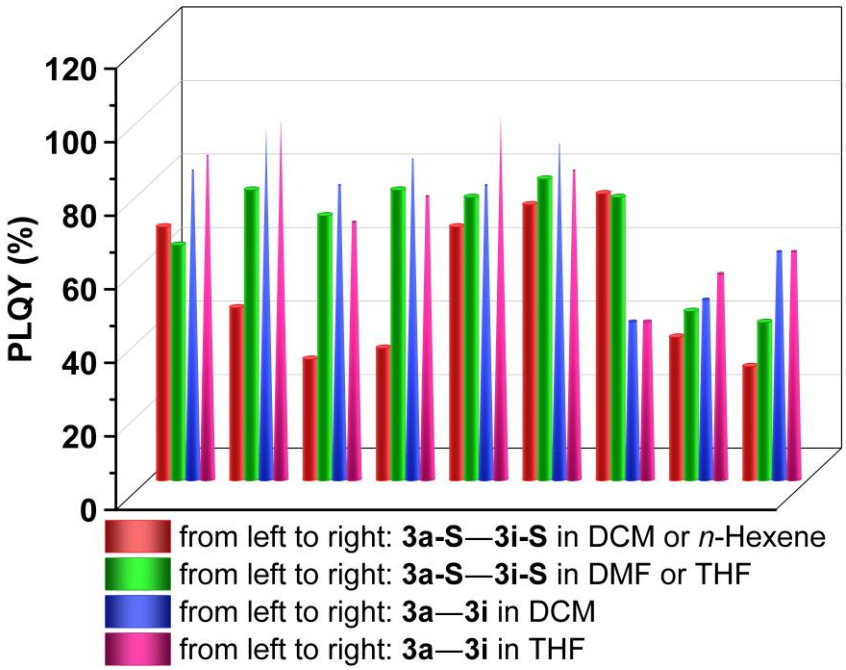


**Fig. S28** The photoluminescence quantum yields (PLQYs) of the luminogens **3a**–**3i** and sulfuric ones **3a-S**–**3i-S**. The data of **3a-S**–**3i-S** are obtained from the recent literatures.[S1, S2]

## 6. Thermal stability and Photostability test data

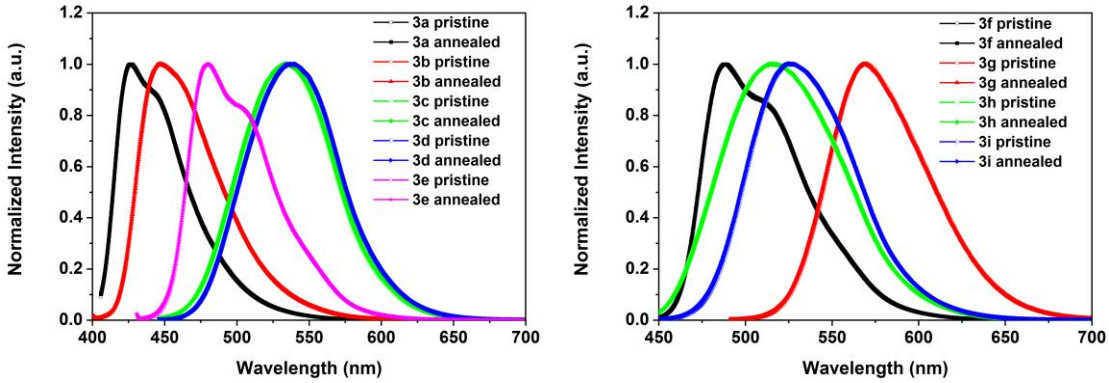


**Fig. S29** Fluorescence spectra of the pristine and annealed **3a**–**3i** in DCM.

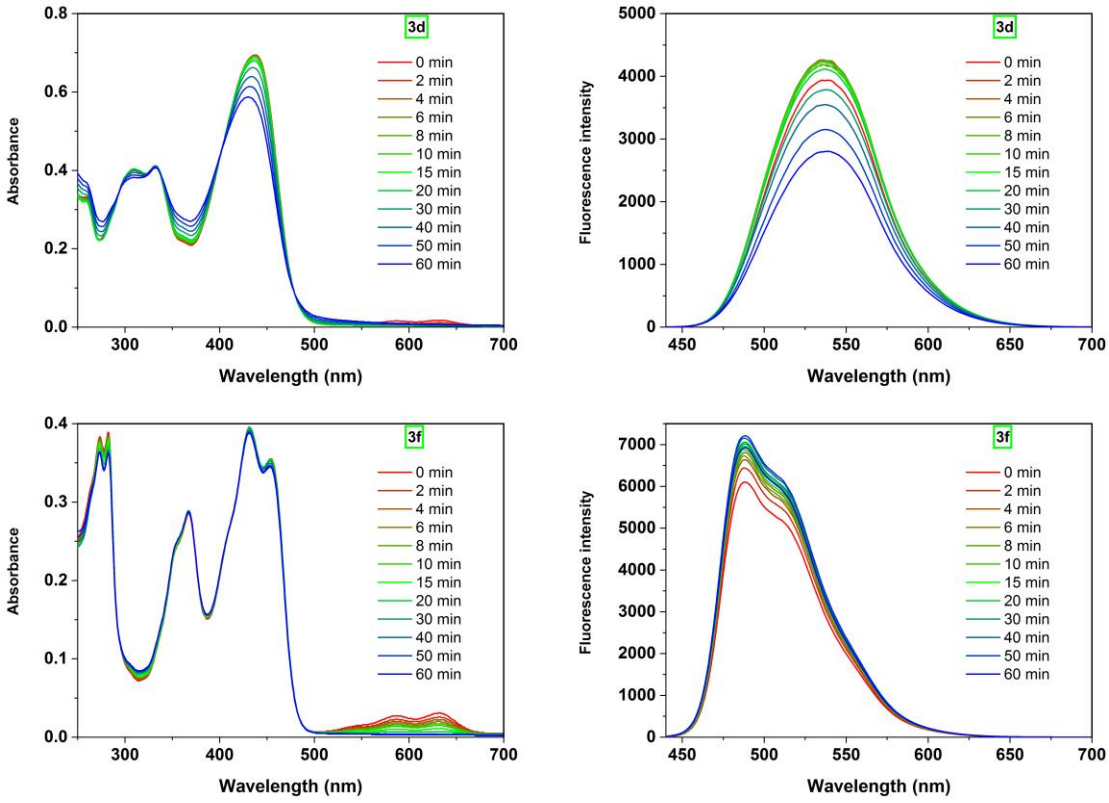


**Fig. S30** Absorption and fluorescence spectra of air-saturated **3d** and **3f** solutions in $CH_2Cl_2$ ($5.0 \times 10^{-6}$ M) after UV exposure (365 nm).

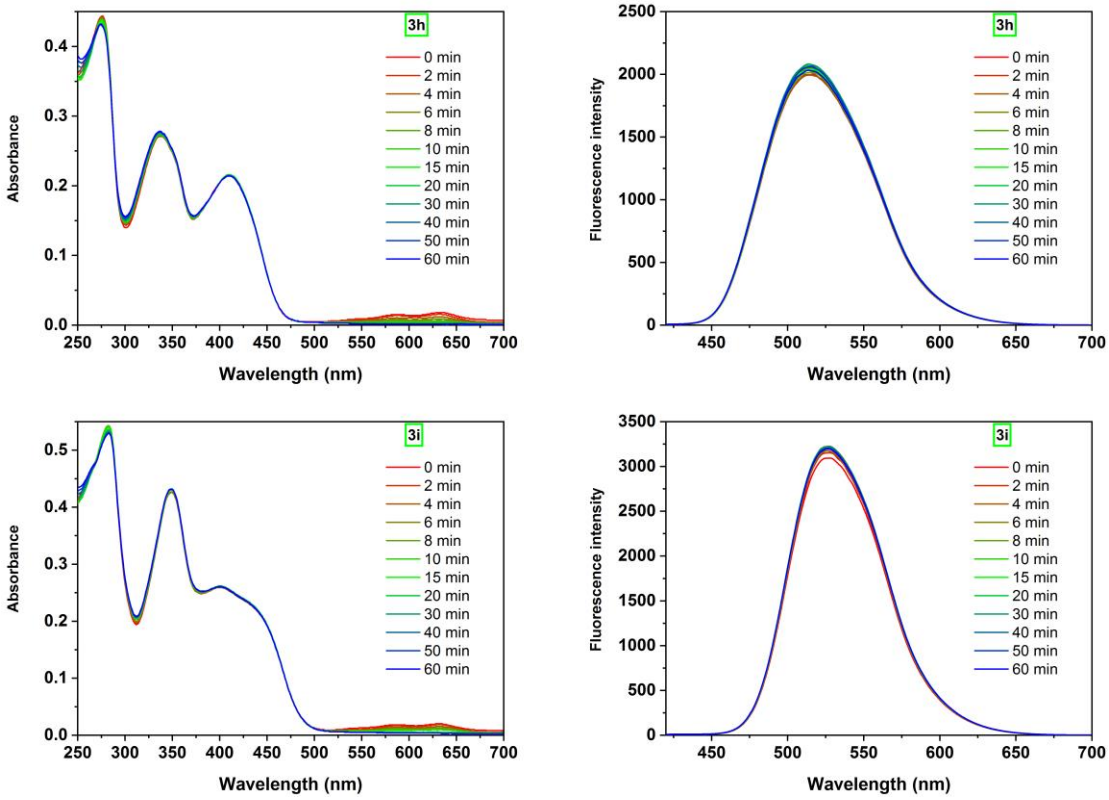


**Fig. S31** Absorption and fluorescence spectra of air-saturated **3h** and **3i** solutions in $CH_2Cl_2$ ($5.0 \times 10^{-6}$ M) after UV exposure (365 nm).

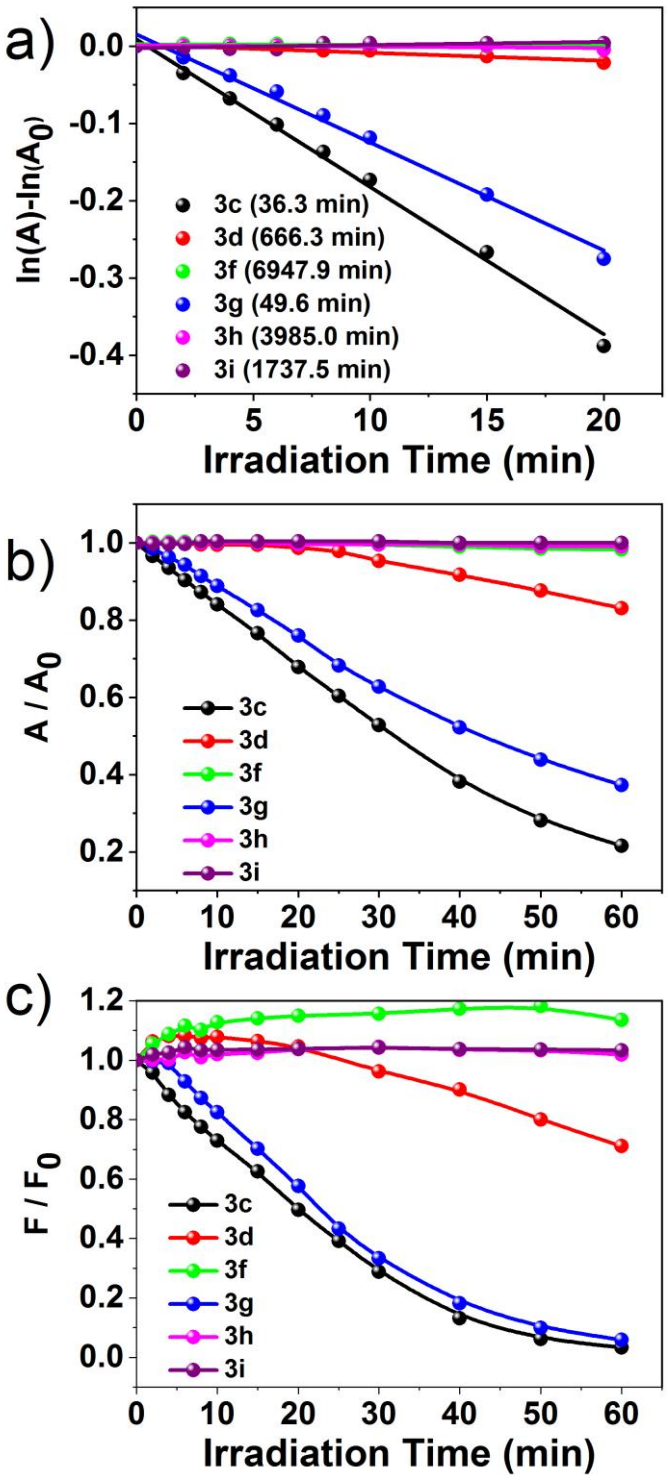


**Fig. S32** a) Pseudo-first-order kinetics analysis of **3c**, **3d** and **3f**–**3i** upon UV irradiation. Profiles of the irradiation time-dependent absorption (b) and integrated fluorescence intensity (c) under irradiation at 365 nm (8 W) in air-saturated DCM.

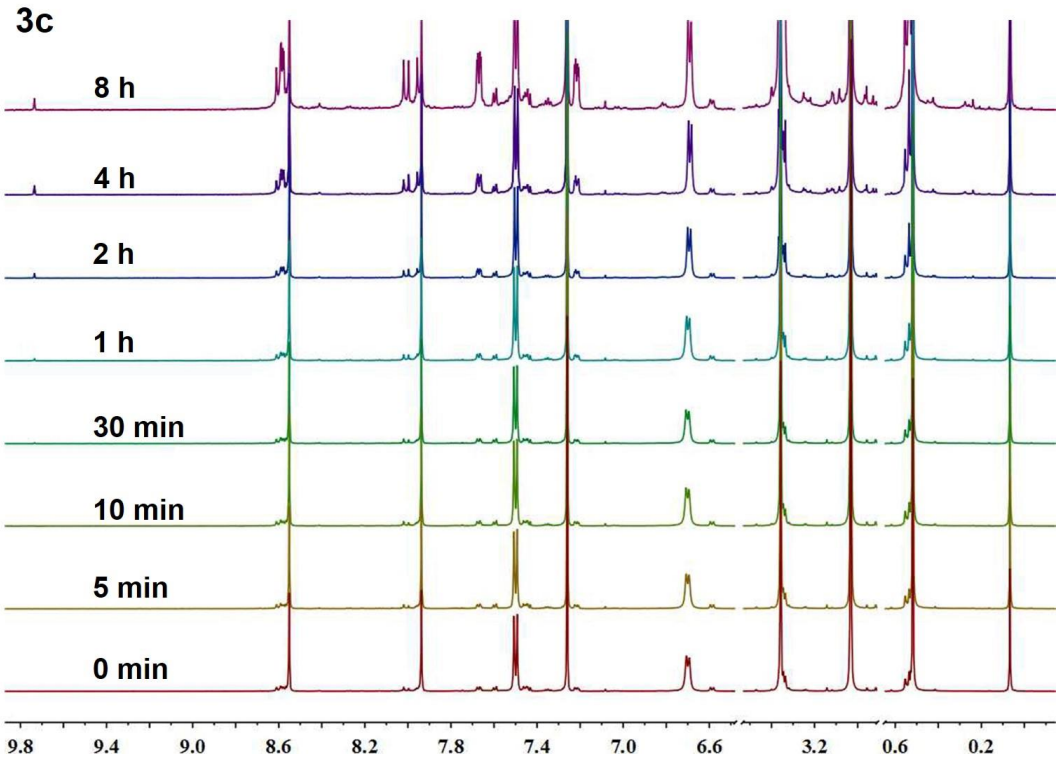


**Fig. S33** $^{1}$H NMR spectral variation (partial aliphatic region is omitted for clarity) of **3c** (1.0 mg in 0.6 mL of $CDCl_3$) with 365 nm irradiation at ambient temperature under air.

## 7. SEM images, composites and cell imaging data

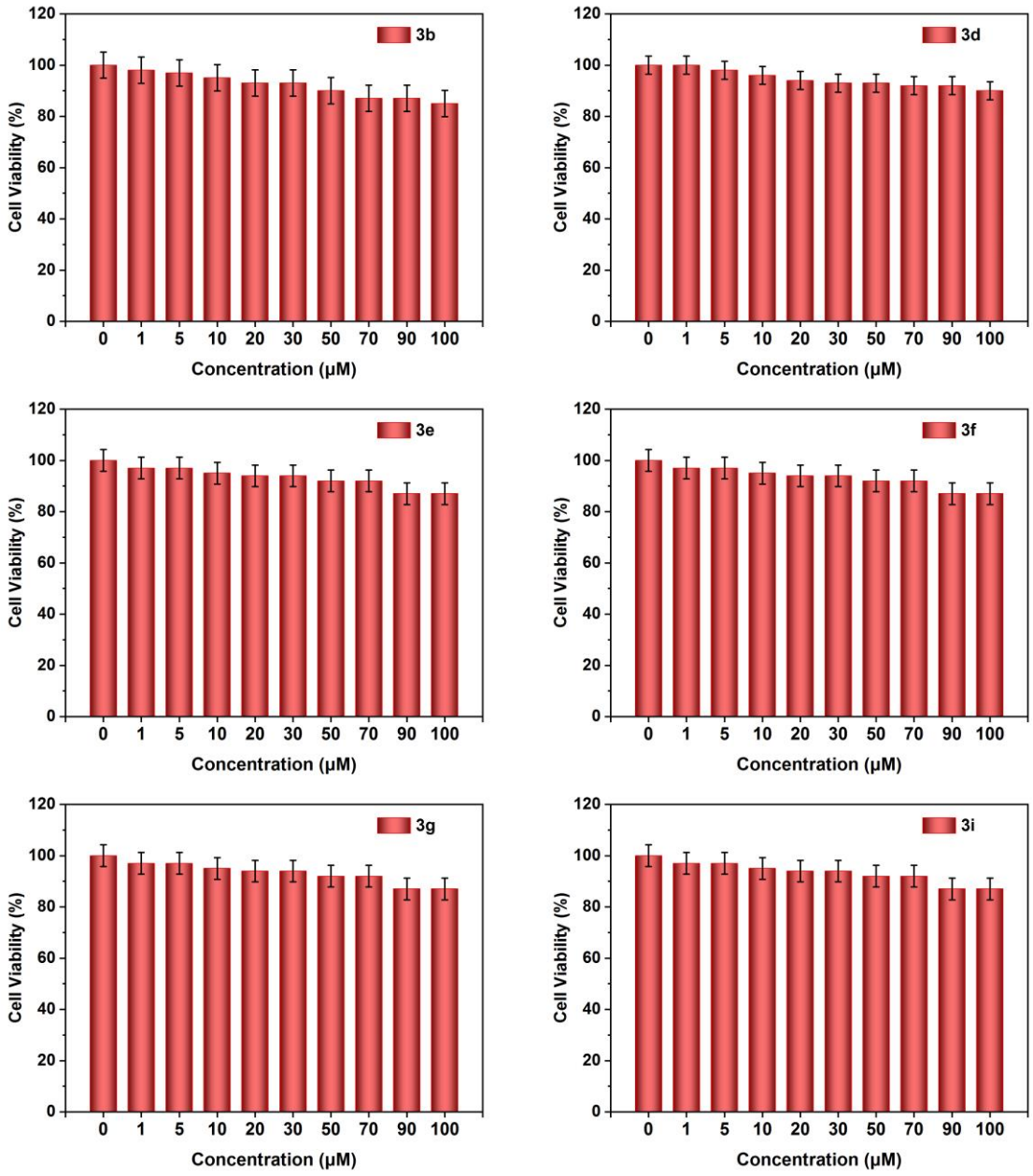


**Fig. S34** Percentage of viable HeLa cells after treatment with **3b**, **3d**, **3e**, **3f**, **3g** and **3i**, respectively, at varied concentrations for 12 h, which is measured by MTT assays.

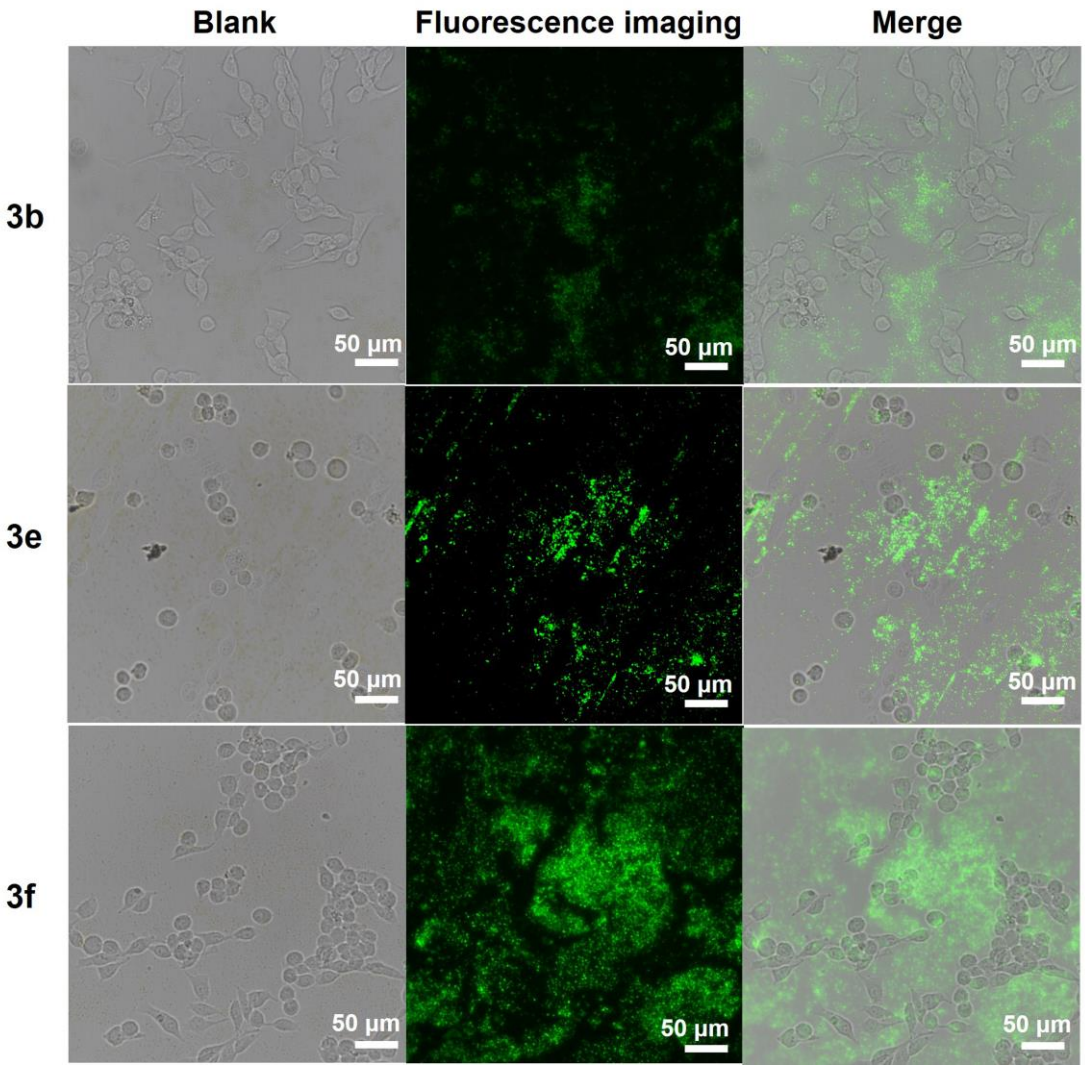


**Fig. S35** Fluorescence images of HeLa cells incubated with **3b**, **3e** and **3f**. The green channel for **3b**, **3e** and **3f** excited at 494 nm and collected in the range of 500–530 nm. The scale bar represents 50 μm.

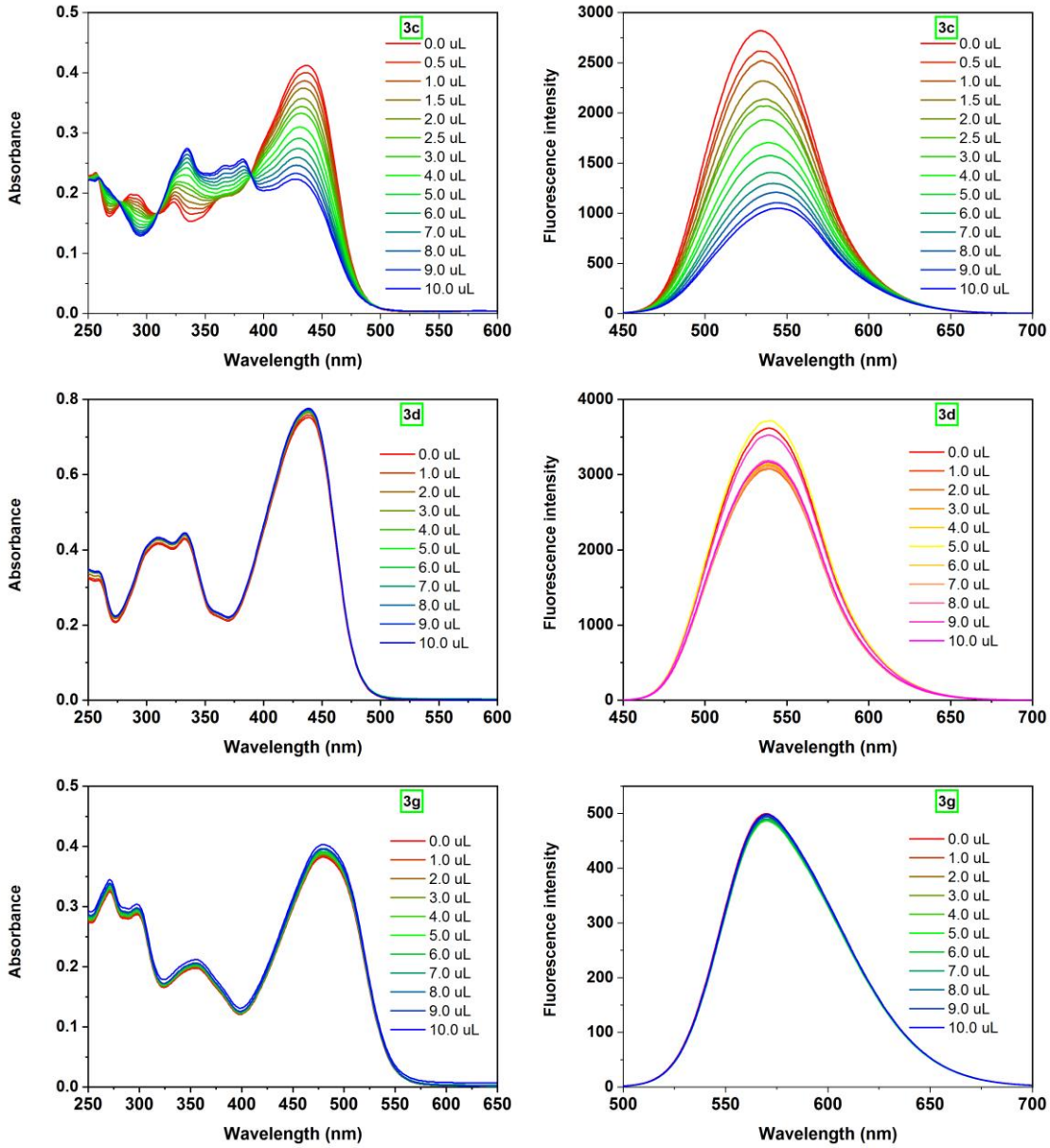


**Fig. S36** Absorption and emission spectra variation of compounds **3c**, **3d** and **3g** (5.0 $\times 10^{-6}$ mol $L^{-1}$) recorded upon addition of various concentrations of $HBF_4$ in DCM.

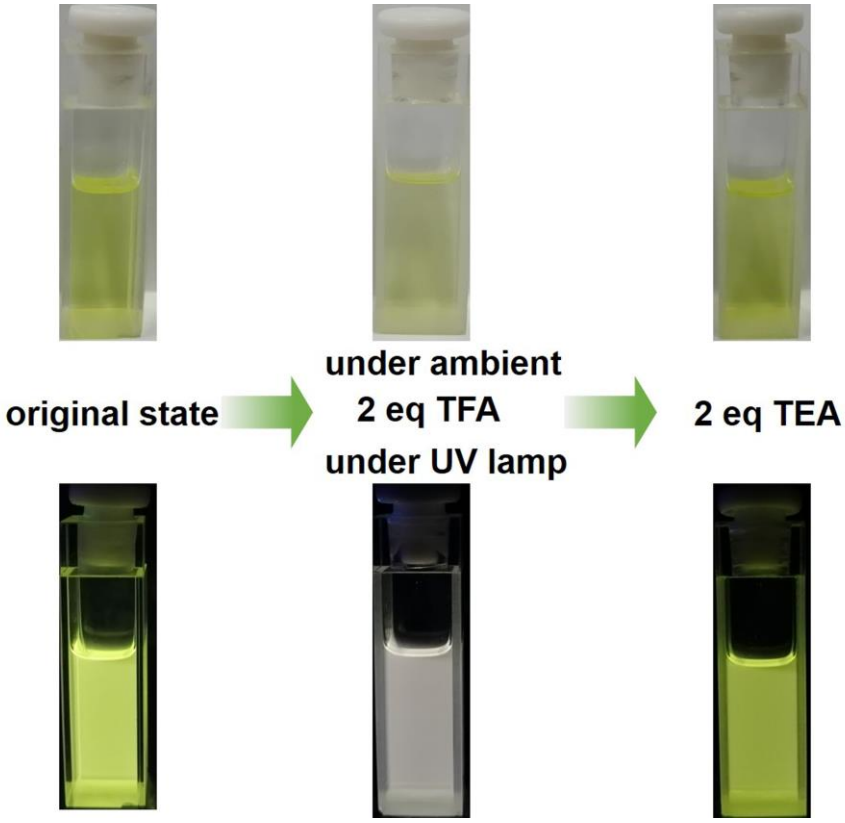


**Fig. S37** Photographs of **3c** solution before adding TFA (left), after adding TFA (central), and then adding TEA (right).

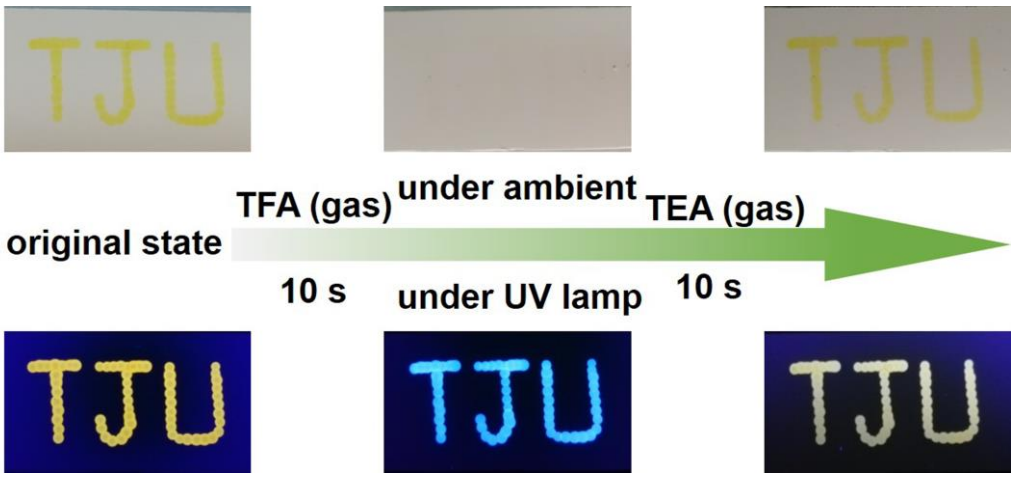


**Fig. S38** Photographs of **3c** on a silica support under ambient (top) and UV (bottom) light observed upon exposure in organic acid and base vapors.

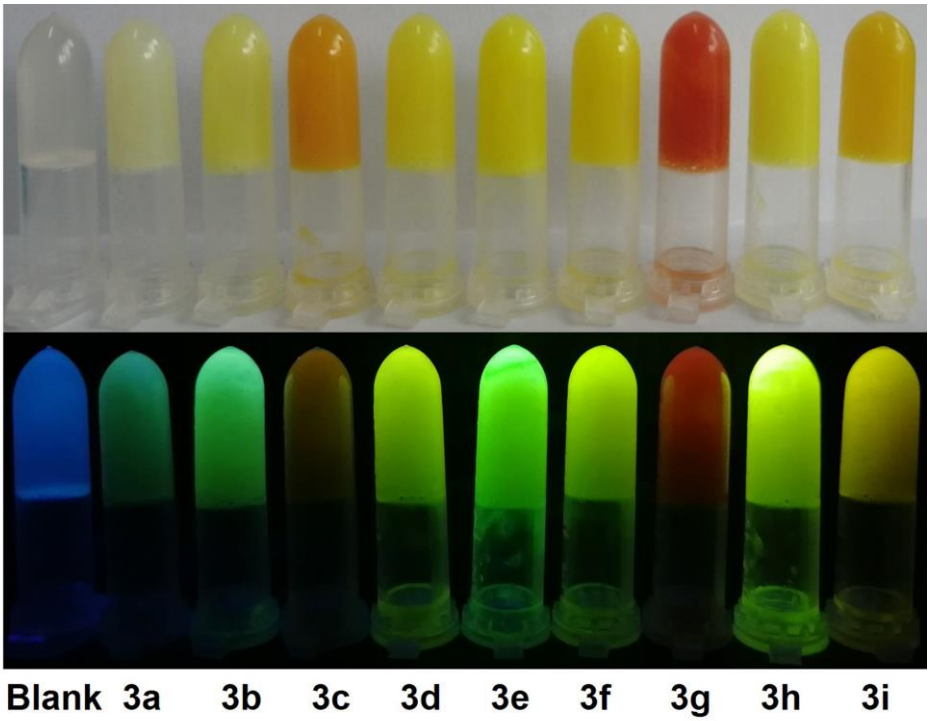


**Fig. S39** Photographs of **3a**−**3i** loaded hydrogels (TG-18) in 4 wt‰ taken under ambient light and UV light (365 nm).

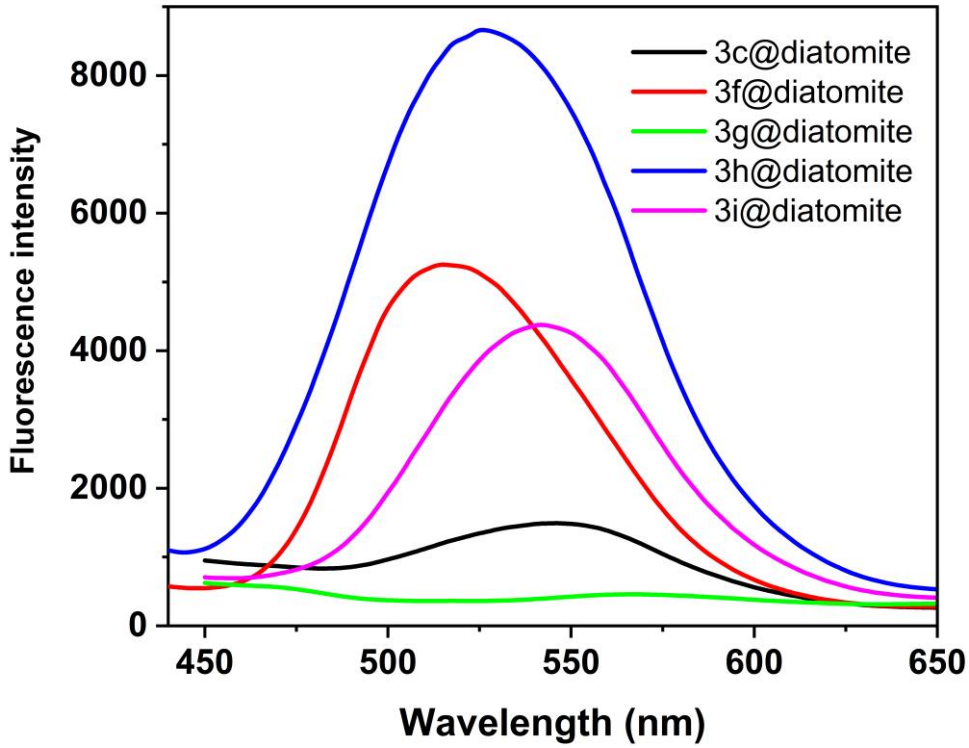


**Fig. S40** The solid-state emission spectra of **3c**@diatomite, **3f**@diatomite, **3g**@diatomite, **3h**@diatomite and **3i**@diatomite measured under room temperature (0.1 mg $g^{-1}$, doping ratio of 0.1 wt‰).

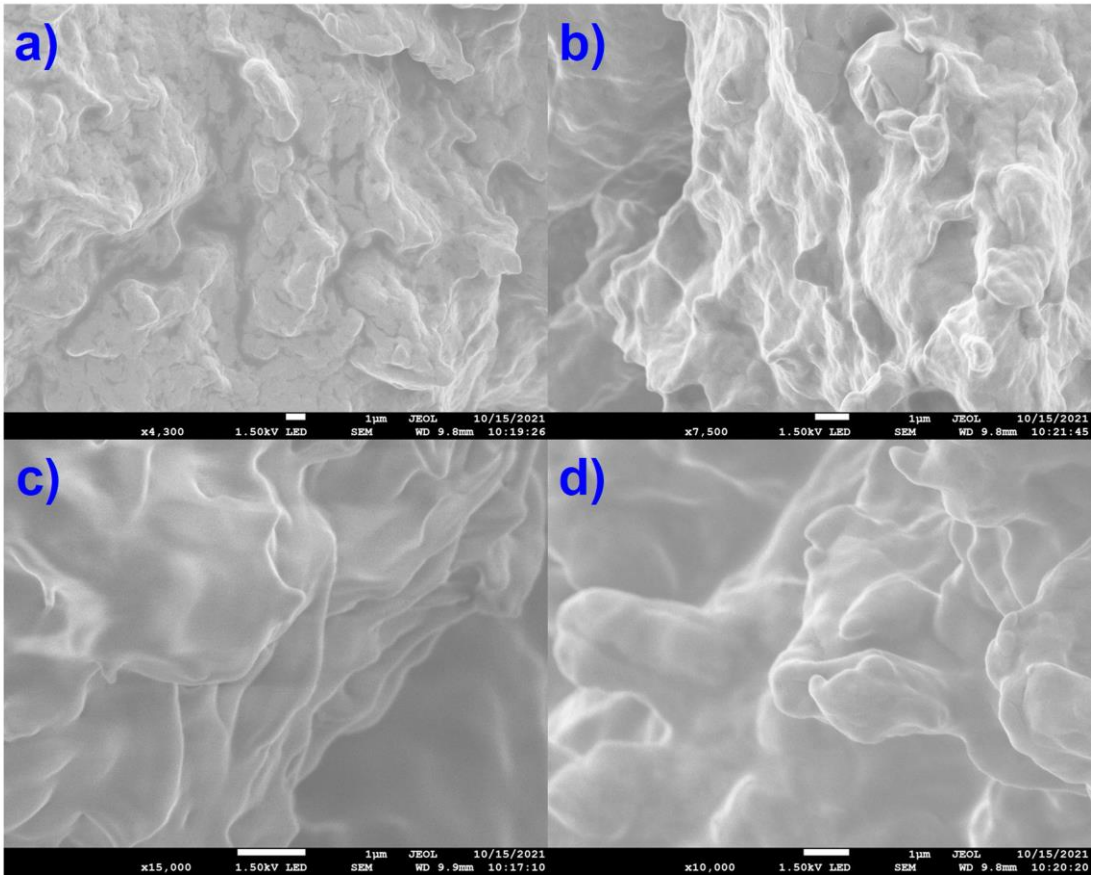


**Fig. S41** SEM images of loaded triglycerol monostearate (TG-18) hydrogel (doping ratio of 4 wt‰).

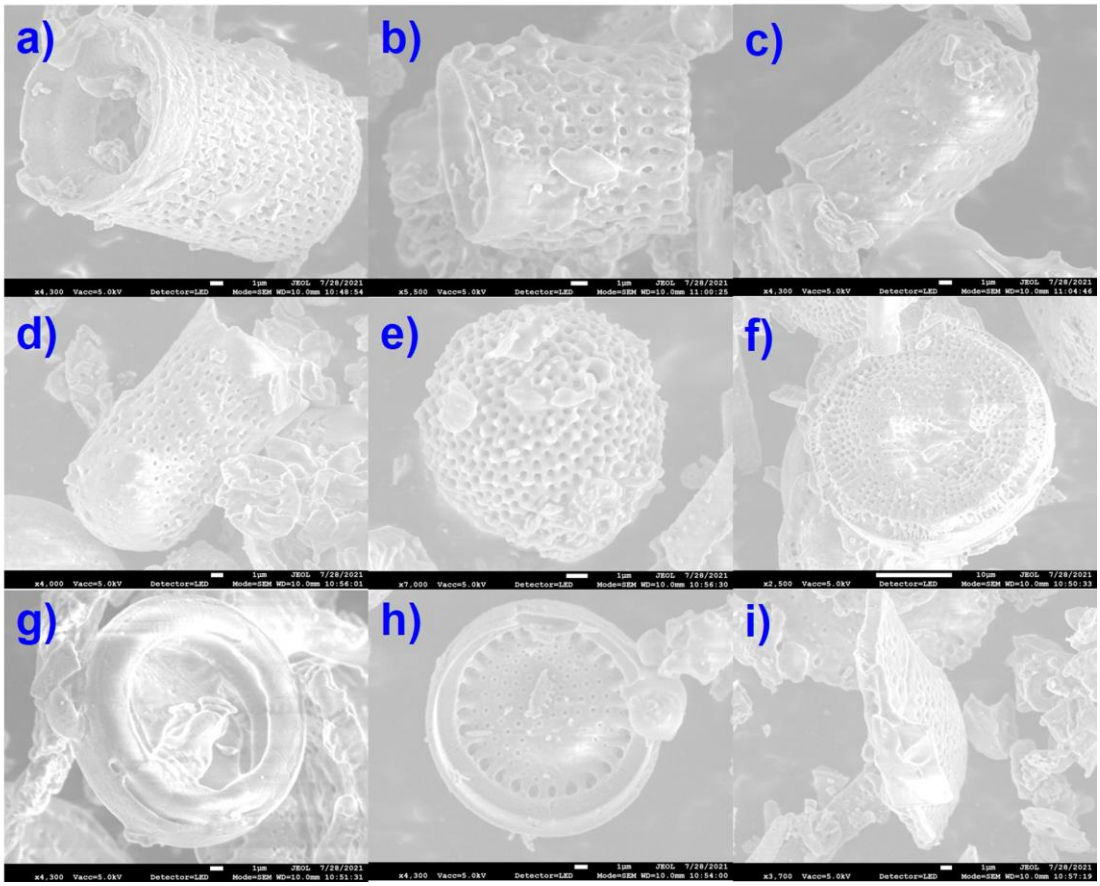


**Fig. S42** SEM images of the loaded pre-processed diatomite (0.1 mg $g^{-1}$, doping ratio of 0.1 wt‰).

## 8. Selected $^{1}$H and $^{13}$C NMR spectra

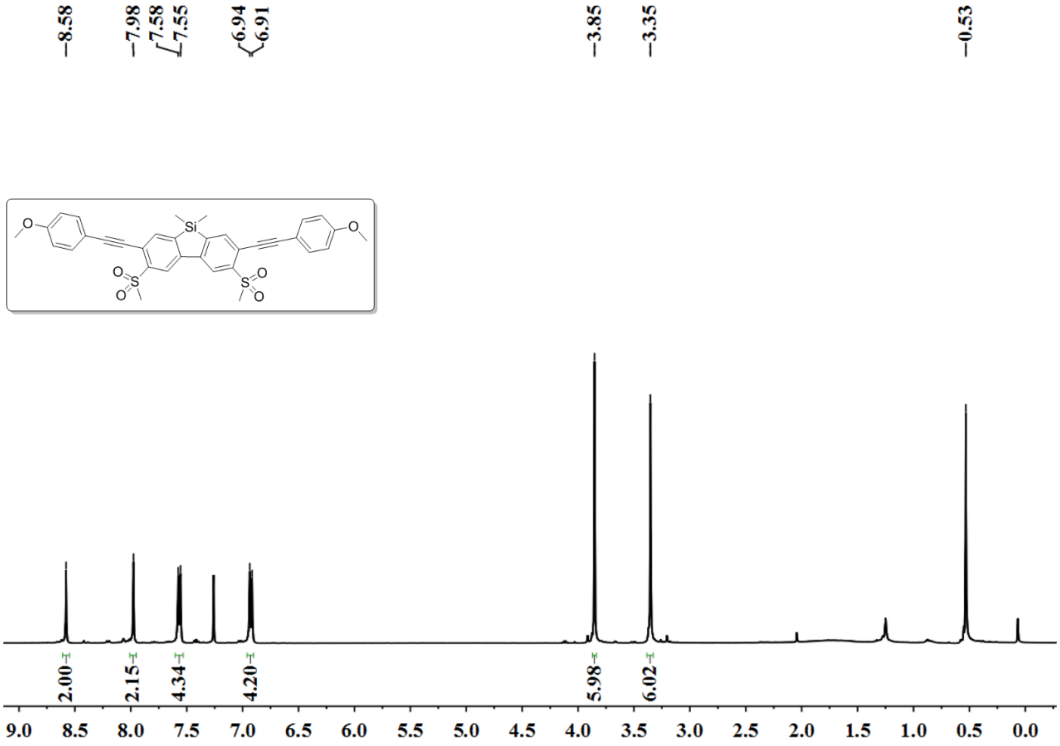


**Fig. S43** $^{1}$H NMR (600 MHz, $CDCl_3$) spectrum for **3a**.

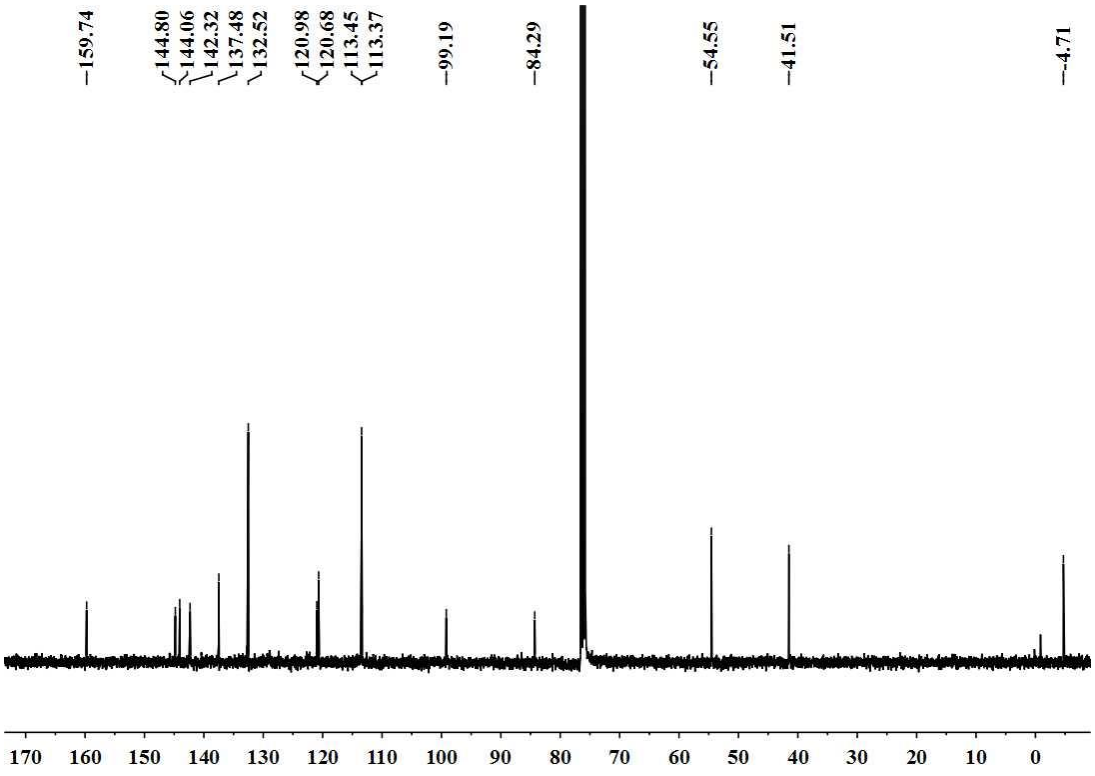


**Fig. S44** $^{13}$C NMR (150 MHz, $CDCl_3$) spectrum for **3a**.

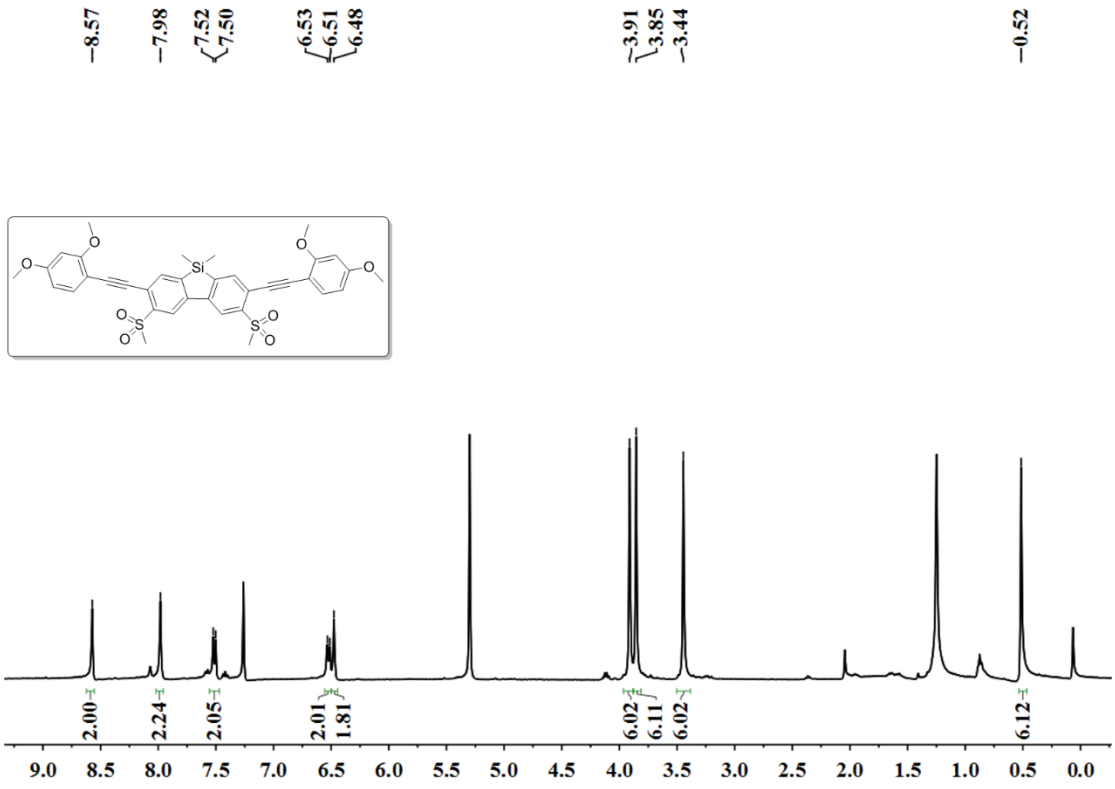


**Fig. S45** $^{1}$H NMR (600 MHz, $CDCl_3$) spectrum for **3b**.

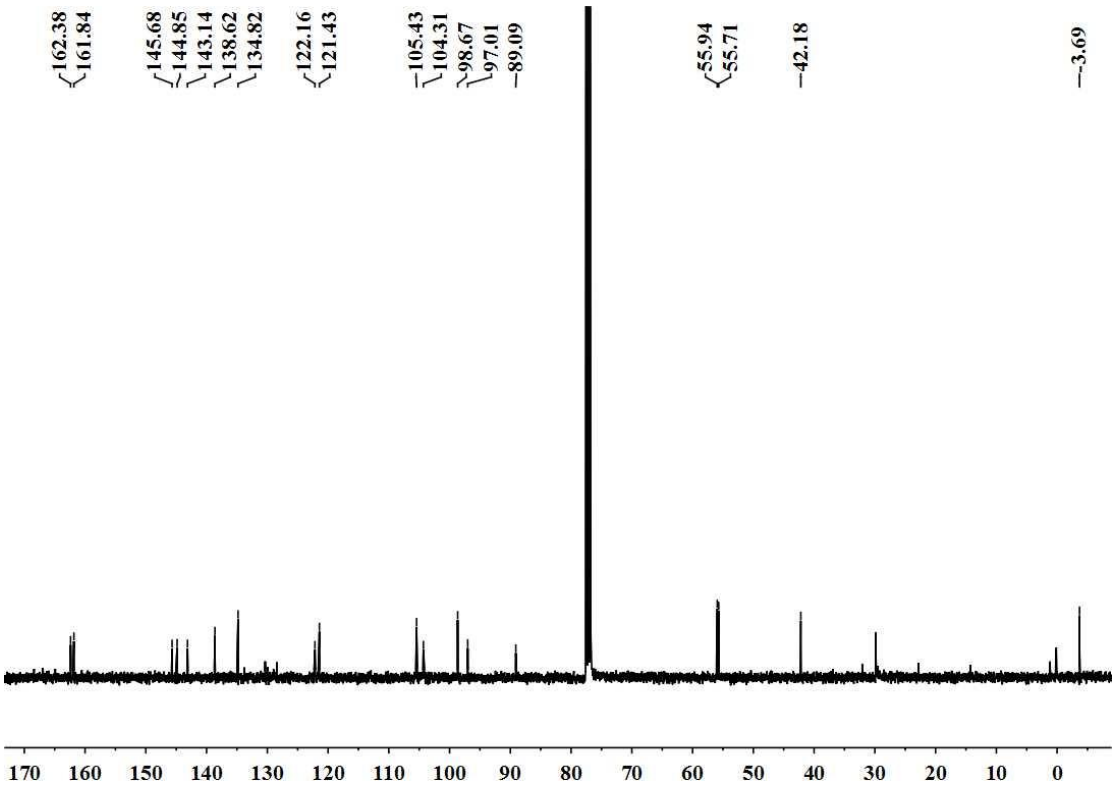


**Fig. S46** $^{13}$C NMR (150 MHz, $CDCl_3$) spectrum for **3b**.

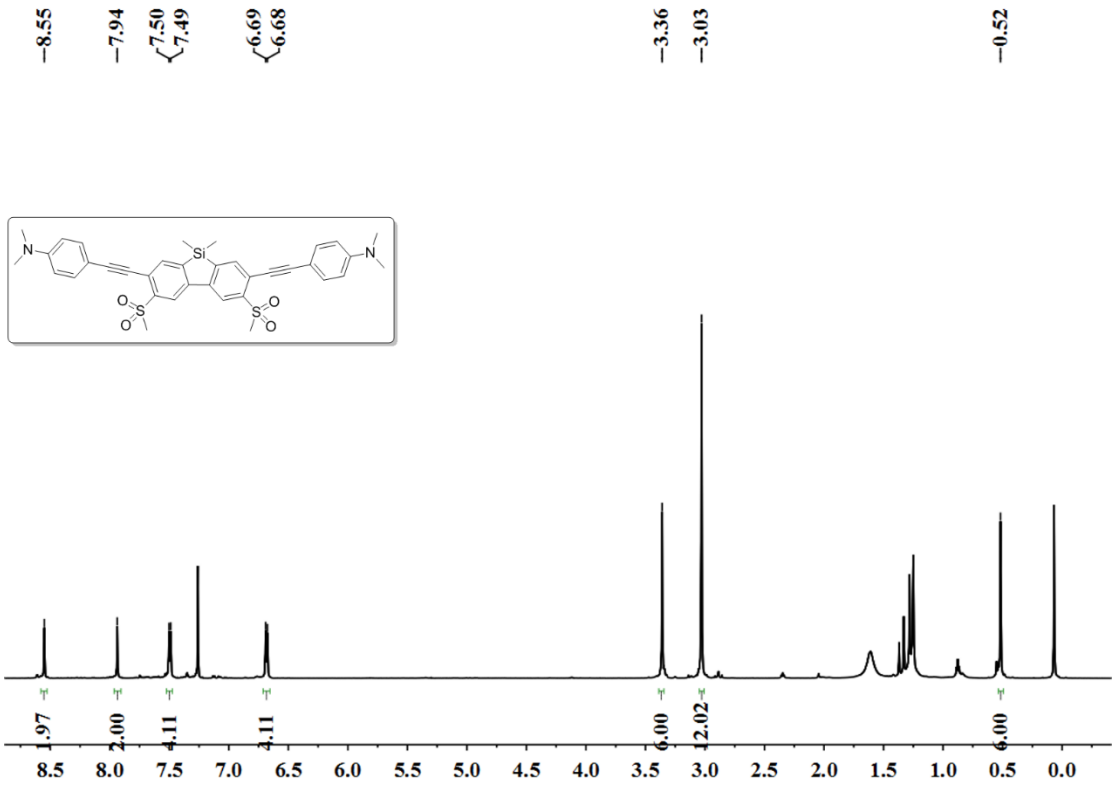


**Fig. S47** $^{1}$H NMR (600 MHz, $CDCl_3$) spectrum for **3c**.

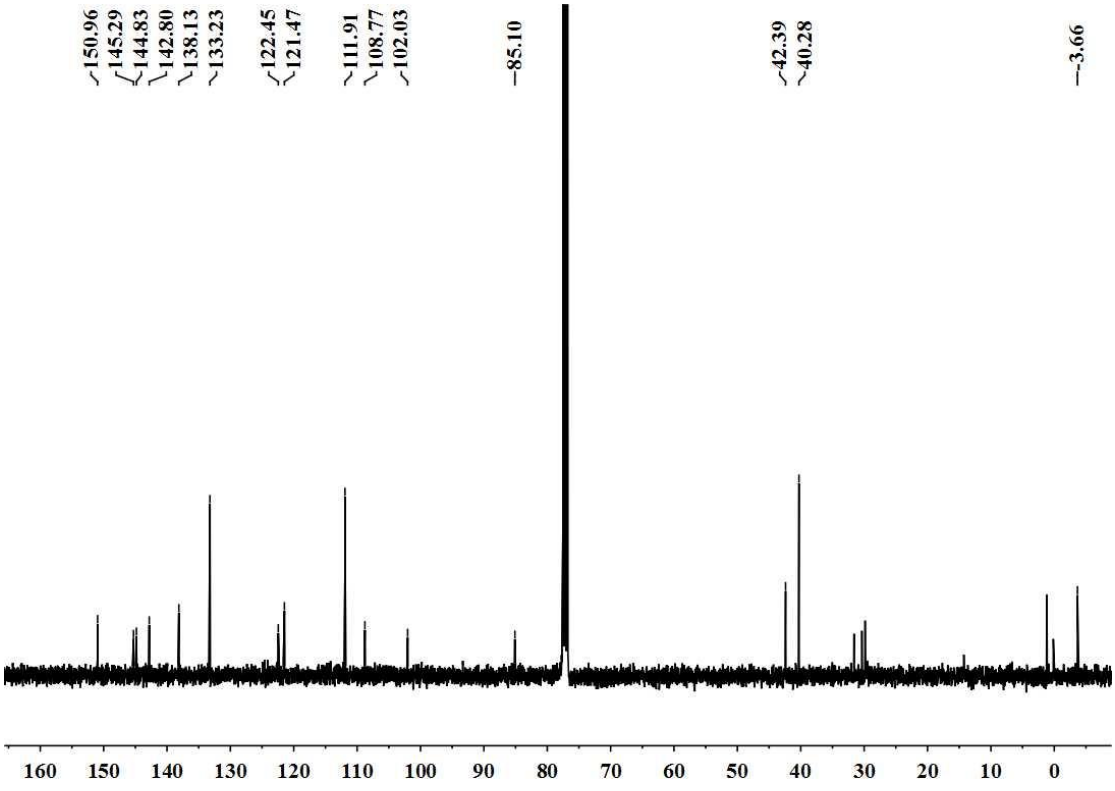


**Fig. S48** $^{13}$C NMR (150 MHz, $CDCl_3$) spectrum for **3c**.

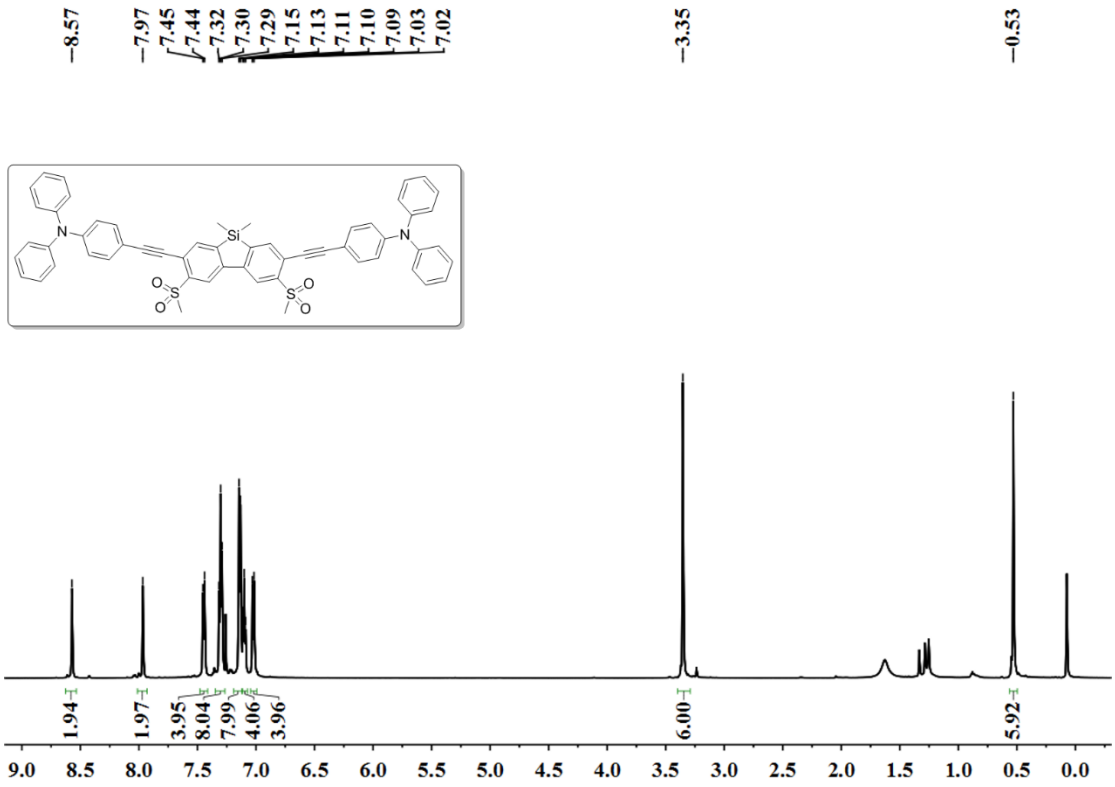


**Fig. S49** $^{1}$H NMR (600 MHz, $CDCl_3$) spectrum for **3d**.

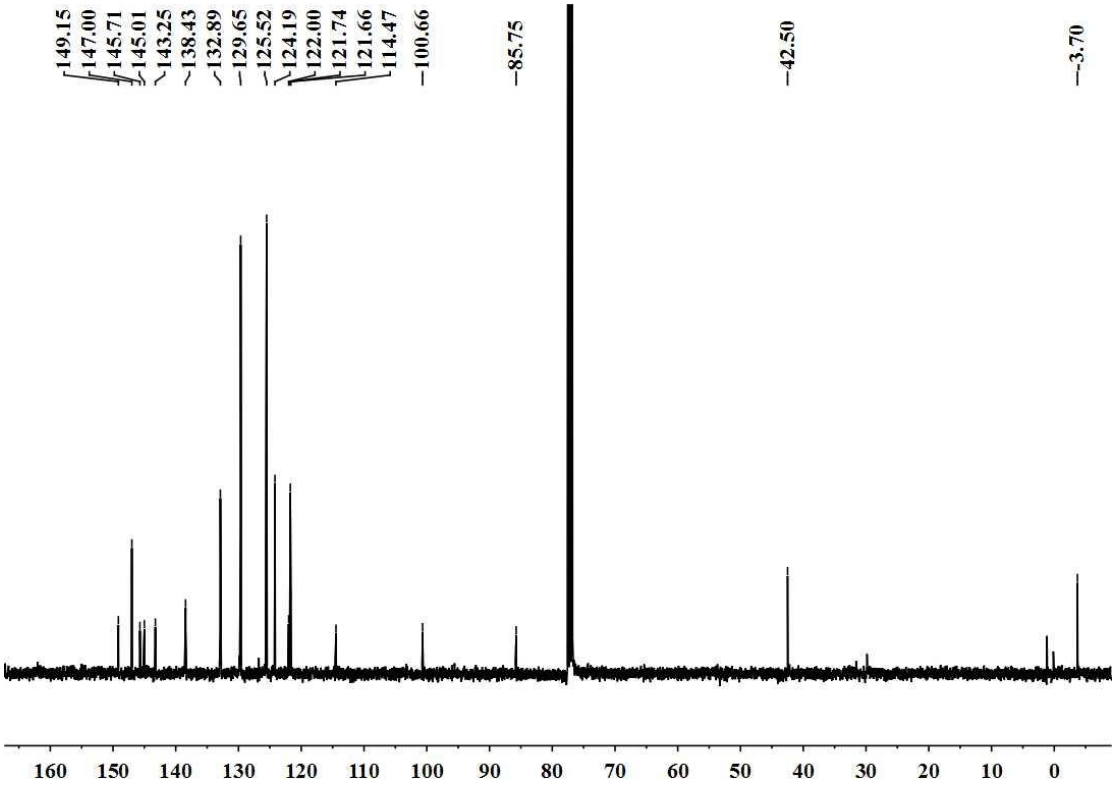


**Fig. S50** $^{13}$C NMR (150 MHz, $CDCl_3$) spectrum for **3d**.

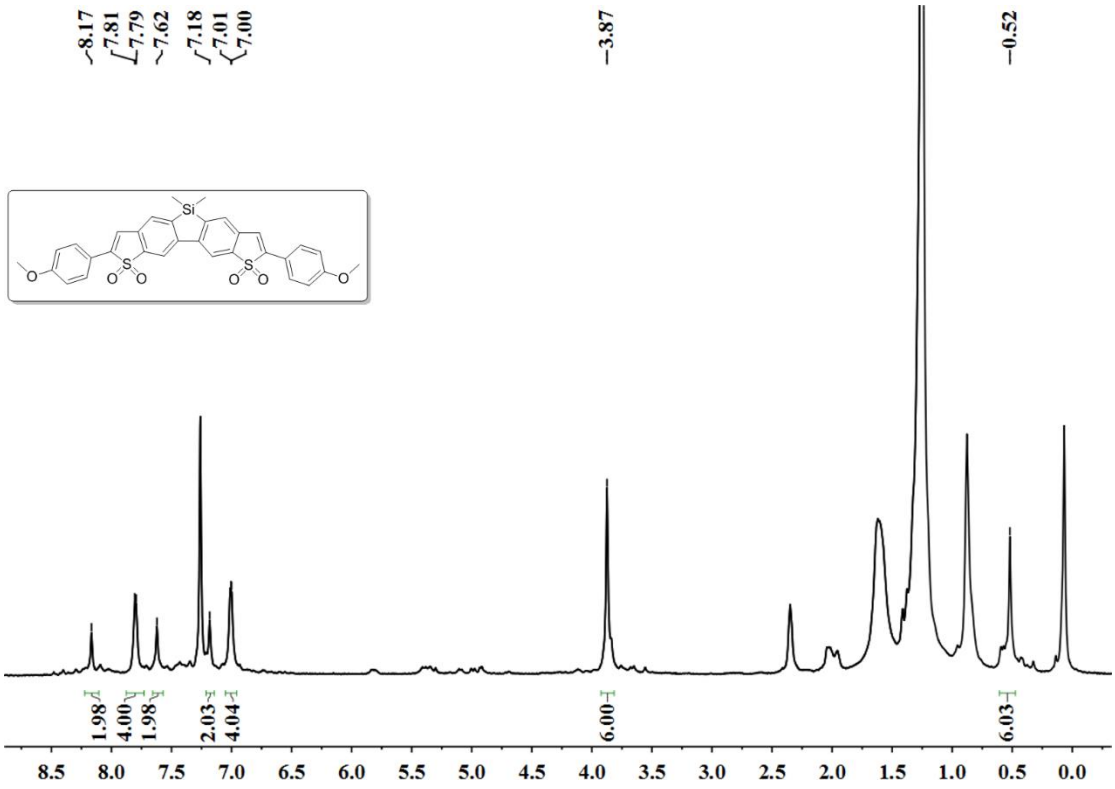


**Fig. S51** $^{1}$H NMR (600 MHz, $CDCl_3$) spectrum for **3e**.

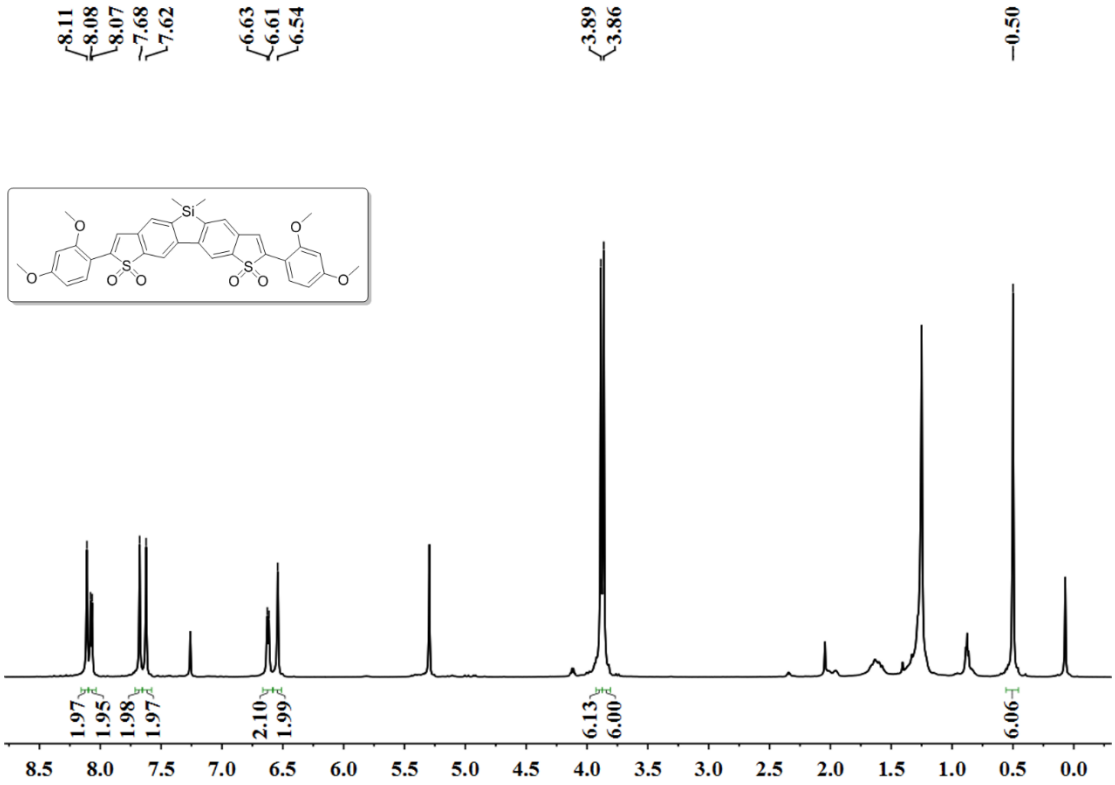


**Fig. S52** $^{1}$H NMR (600 MHz, $CDCl_3$) spectrum for **3f**.

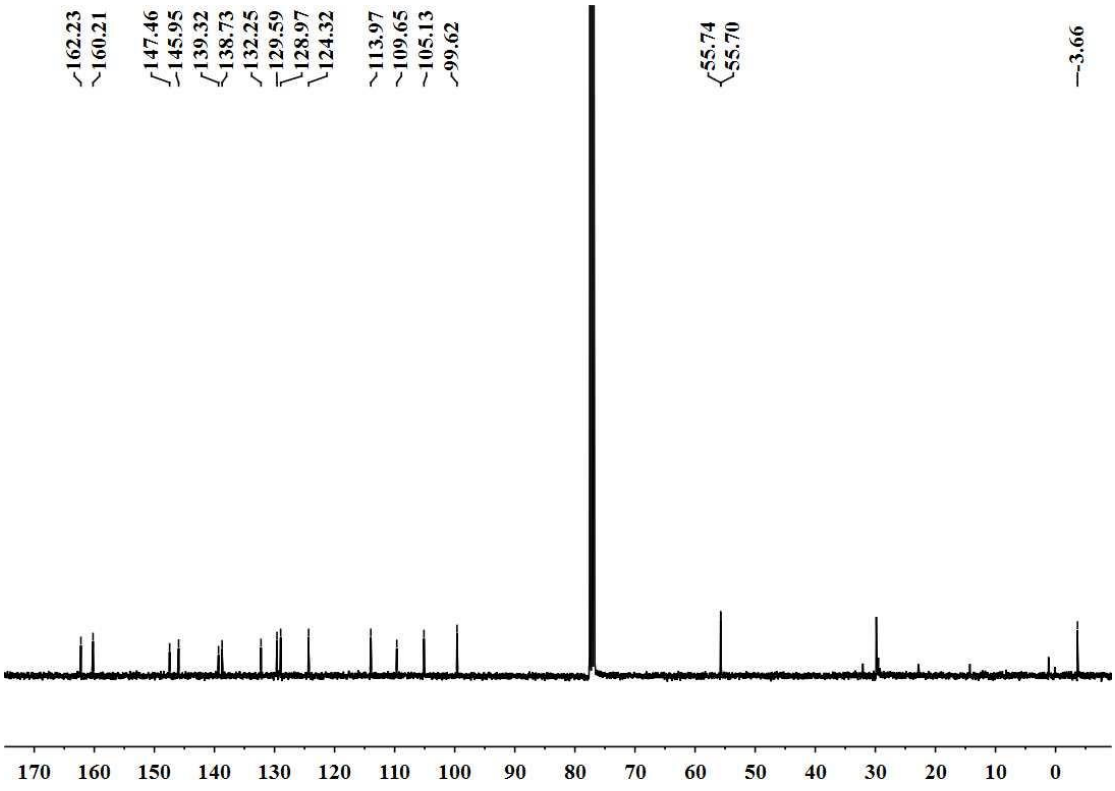


**Fig. S53** $^{13}$C NMR (150 MHz, $CDCl_3$) spectrum for **3f**.

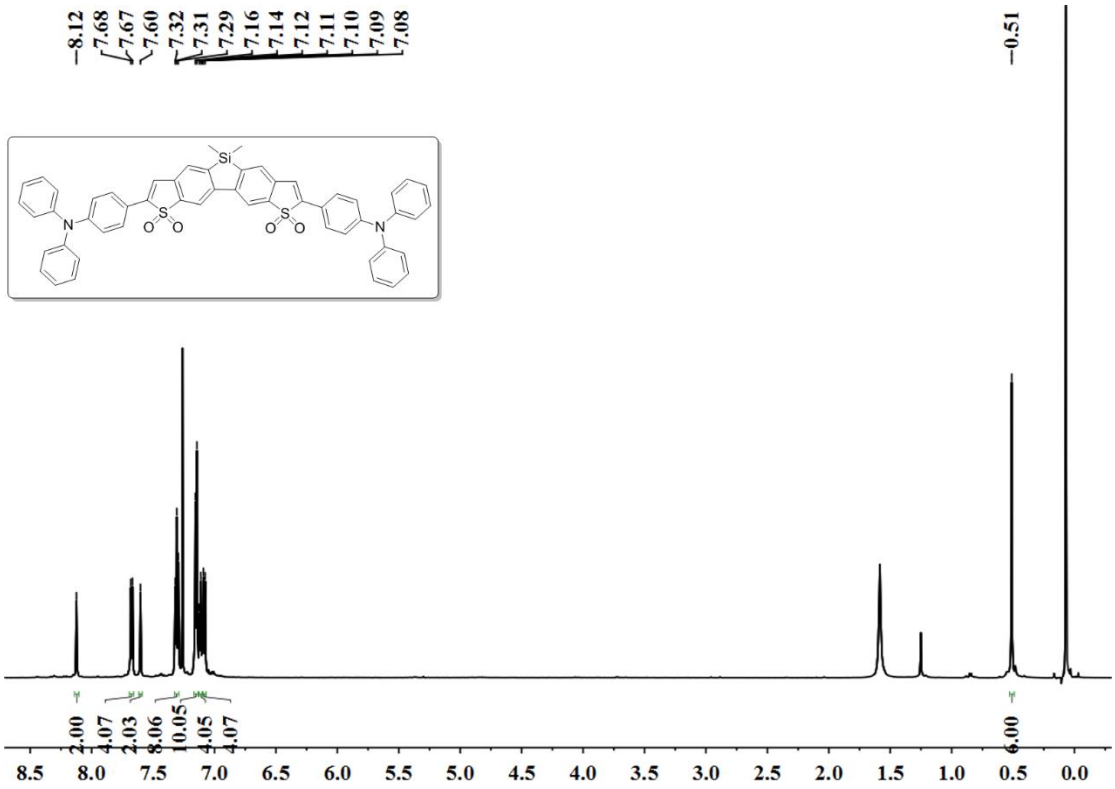


**Fig. S54** $^{1}$H NMR (600 MHz, $CDCl_3$) spectrum for **3g**.

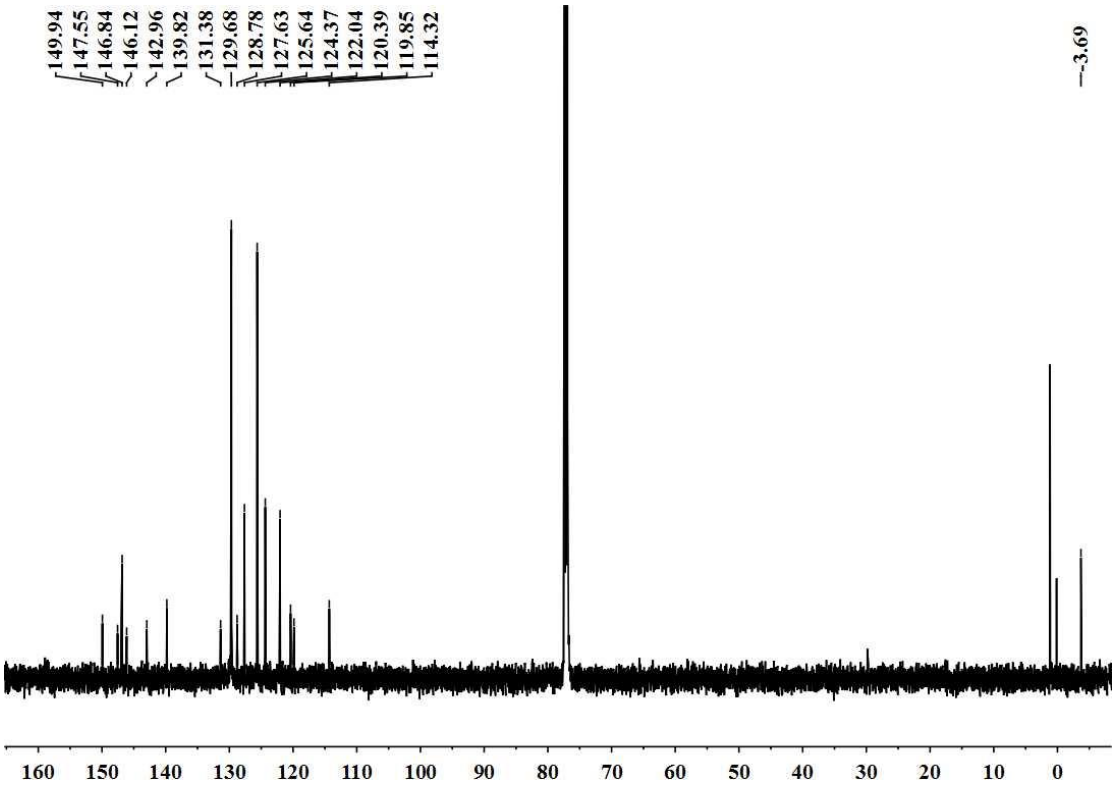


**Fig. S55** $^{13}$C NMR (150 MHz, $CDCl_3$) spectrum for **3g**.

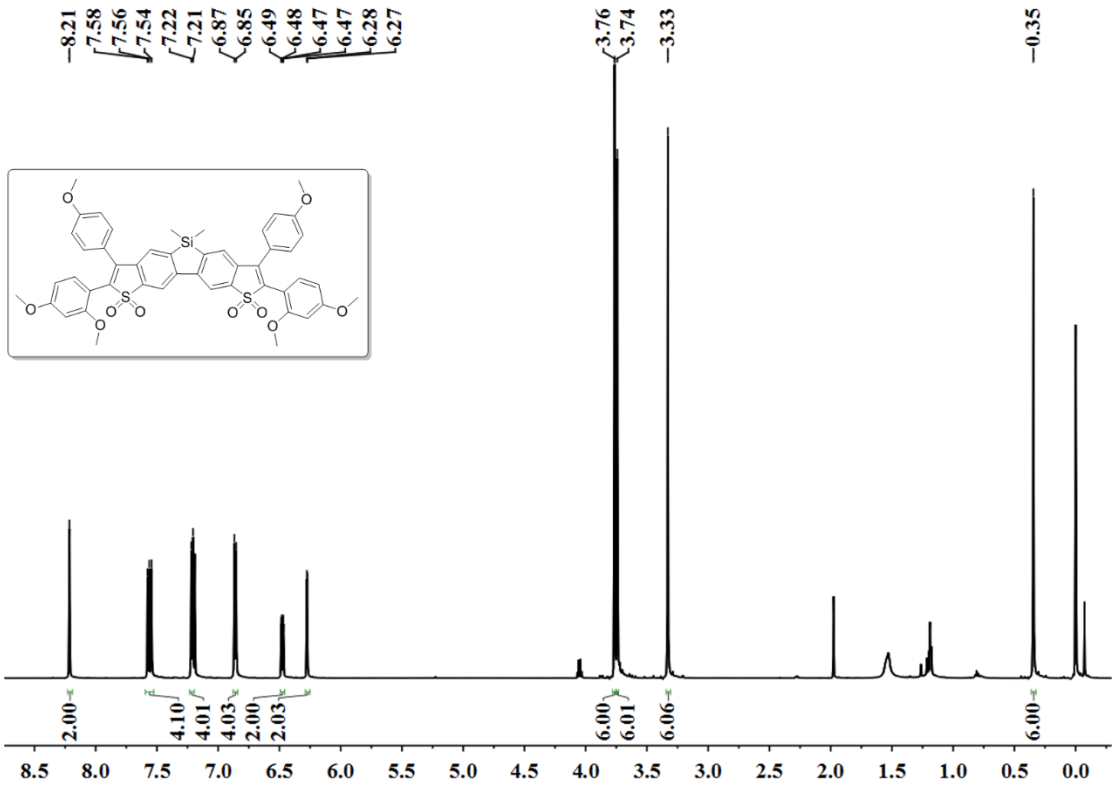


**Fig. S56** $^{1}$H NMR (600 MHz, $CDCl_3$) spectrum for **3h**.

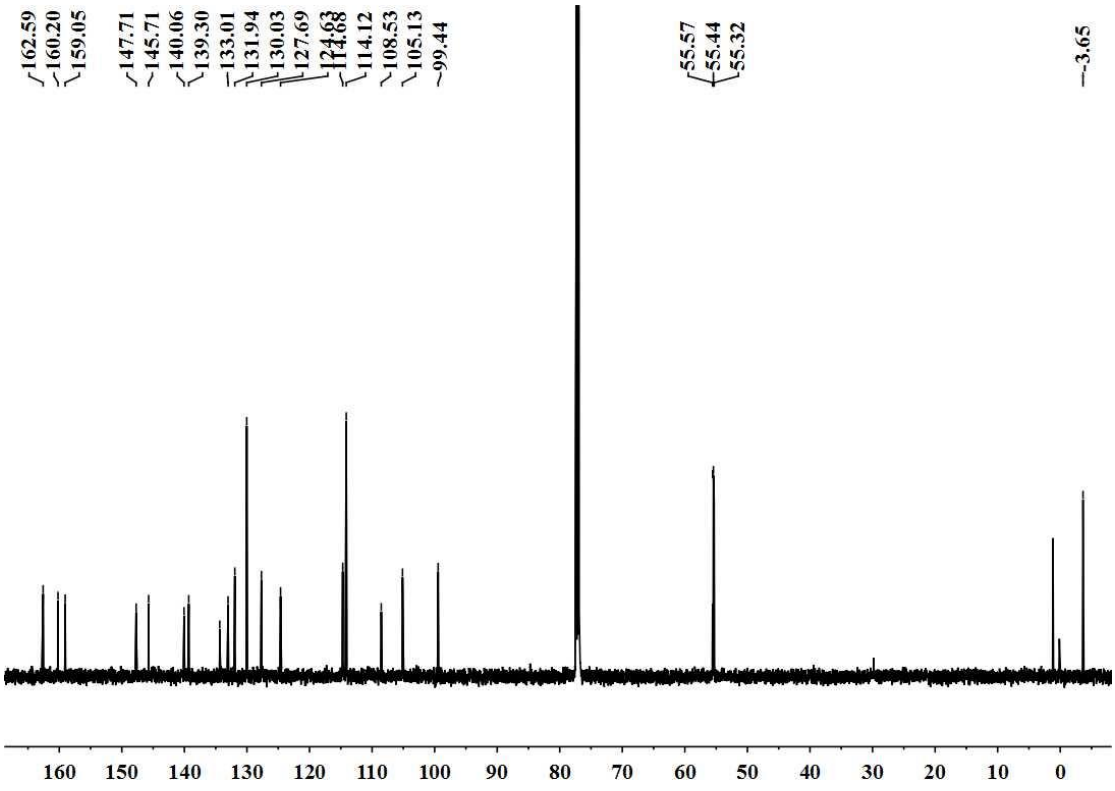


**Fig. S57** $^{13}$C NMR (150 MHz, $CDCl_3$) spectrum for **3h**.

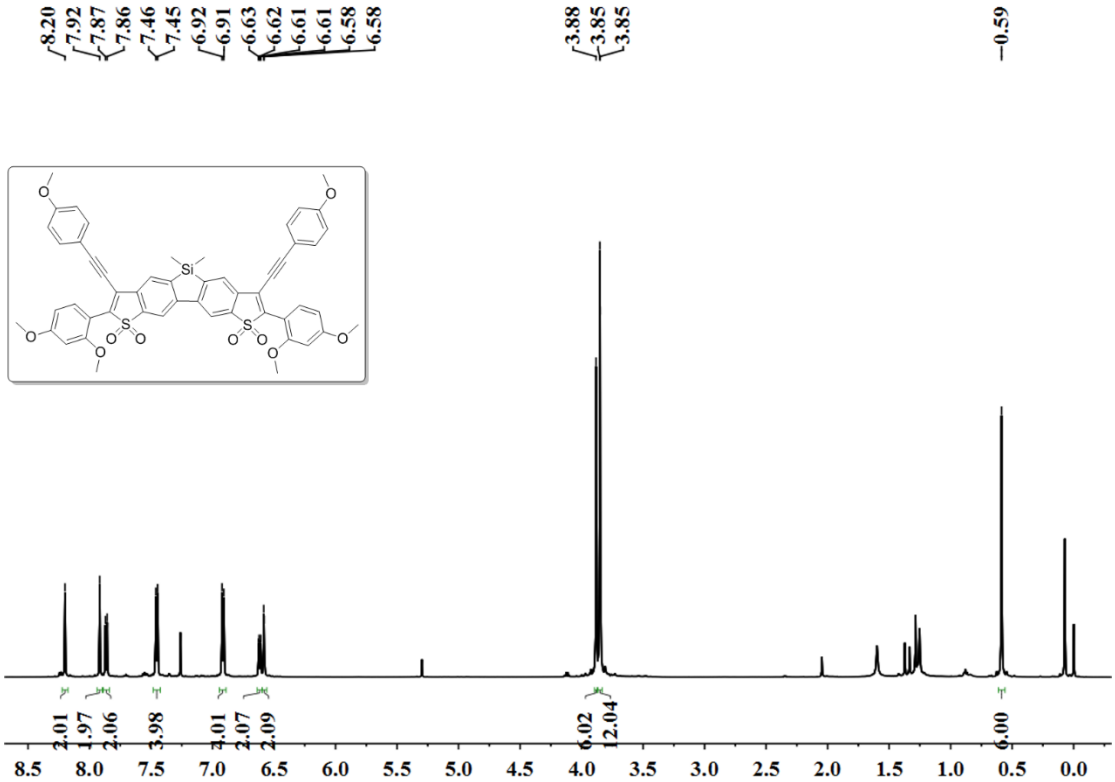


**Fig. S58** $^{1}$H NMR (600 MHz, $CDCl_3$) spectrum for **3i**.

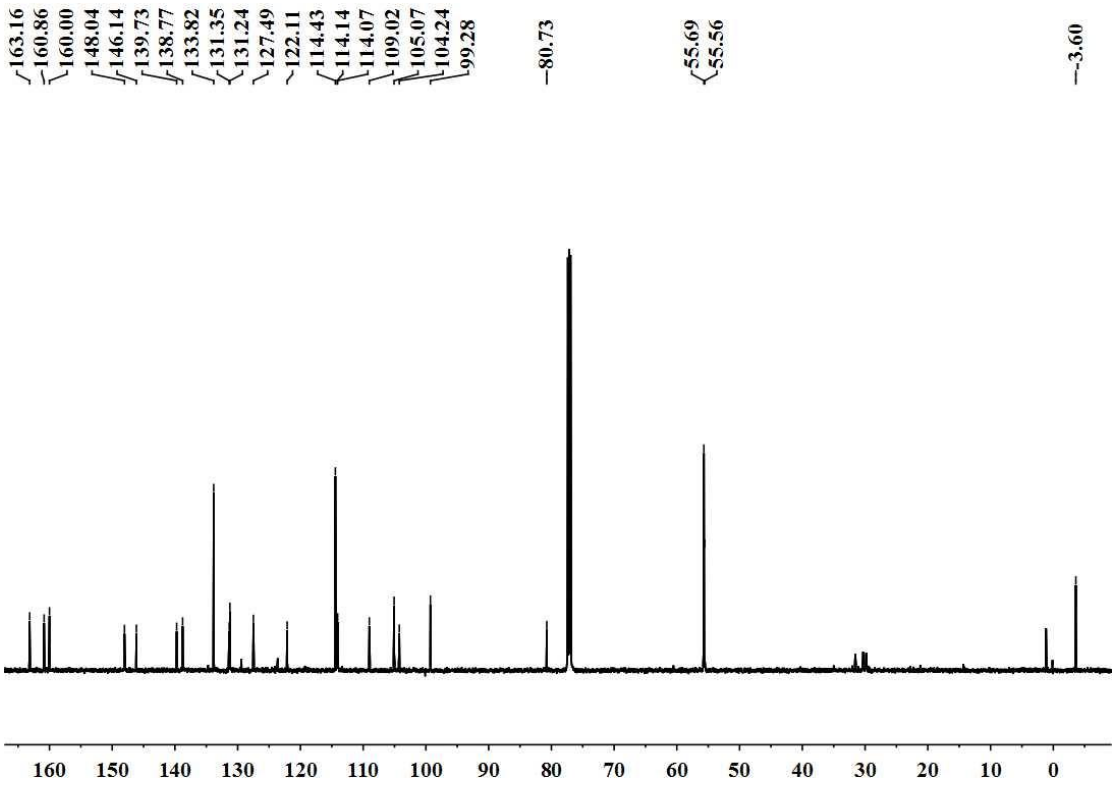


**Fig. S59** $^{13}C$ NMR (150 MHz, $CDCl_3$) spectrum for **3i**.

## 9. References


[S1] G. Gou, Z. Zhang, B. Yuan, T. Fan and L. Li, *Dyes Pigments*, 2021, **194**, 109642.

[S2] G. Gou, Z. Zhang, T. Fan, L. Fang and L. Li, *Chinese Chem. Lett.*, 2022, **33**, 4306–4312.

[S3] M. J. Frisch, G. W. Trucks, H. B. Schlegel, G. E. Scuseria, M. A. Robb, J. R. Cheeseman, G. Scalmani, V. Barone, G. A. Petersson, H. Nakatsuji, X. Li, M. Caricato, A. V. Marenich, J. Bloino, B. G. Janesko, R. Gomperts, B. Mennucci, H. P. Hratchian, J. V. Ortiz, A. F. Izmaylov, J. L. Sonnenberg, D. Williams-Young, F. Ding, F. Lipparini, F. Egidi, J. Goings, B. Peng, A. Petrone, T. Henderson, D. Ranasinghe, V. G. Zakrzewski, J. Gao, N. Rega, G. Zheng, W. Liang, M. Hada, M. Ehara, K. Toyota, R. Fukuda, J. Hasegawa, M. Ishida, T. Nakajima, Y. Honda, O. Kitao, H. Nakai, T. Vreven, K. Throssell, J. A. Montgomery, J. E. P. Jr., F. Ogliaro, M. J. Bearpark, J. J. Heyd, E. N. Brothers, K. N. Kudin, V. N. Staroverov, T. A. Keith, R. Kobayashi, J. Normand, K. Raghavachari, A. P. Rendell, J. C. Burant, S. S. Iyengar, J. Tomasi, M. Cossi, J. M. Millam, M. Klene, C. Adamo, R. Cammi, J. W. Ochterski, R. L. Martin, K. Morokuma, O. Farkas, J. B. Foresman and D. J. Fox, *Gaussian 16, Revision A.03*, Gaussian, Inc., Wallingford CT, 2016..

[S4] O. V. Dolomanov, L. J. Bourhis, R. J. Gildea, J. A. Howard and H. Puschmann, *J. Appl. Crystallogr.*, 2009, **42**, 339–341.

[S5] N. G. Connelly and W. E. Geiger, *Chem. Rev.*, 1996, **96**, 877–910.

[S6] A. D. Becke, *Phys. Rev. A*, 1988, **38**, 3098–3100.

[S7] A. D. Becke, *J. Chem. Phys.*, 1993, **98**, 5648–5652.

[S8] S. Miertuš, E. Scrocco and J. Tomasi, *Chem. Phys.*, 1981, **55**, 117–129.